Basin Research (2008) **20**, 119–142, doi: 10.1111/j.1365-2117.2007.00345.x

Basin modelling of the Limón Back-arc Basin (Costa Rica): burial history and temperature evolution of an island arc-related basin-system

C. Brandes,* A. Astorga,† R. Littke‡ and J. Winsemann*

*Institut für Geologie, Leibniz Universität Hannover, Hannover, Germany
†Escuela Centroamericana de Geología, San José, Costa Rica
‡Lehrstuhl für Geologie, Geochemie und Lagerstätten des Erdöls und der Kohle, Aachen, Germany

ABSTRACT

The Limón back-arc basin belongs to the southern Central American arc-trench system and is situated at the east coast of Costa Rica. The basin-fill consists of Late Cretaceous to Pleistocene sedimentary rocks. A northern and a southern sub-basin can be defined, separated by the E–W-trending Trans Isthmic Fault System. The North Limón Basin is nearly undeformed, whereas the South Limón Basin is characterized by a fold-and-thrust belt. Both sub-basins have a very similar sedimentary fill and can act as a natural laboratory for reconstructing controlling factors of arc-related sedimentary basins as well as the influence of deformation on a basin system. Modelling focused on burial history and temperature evolution. Two-dimensional simulations were carried out with the software PetroMod®. The geohistory curve of the North Limón Basin is overall linear, indicating continuous subsidence. The South Limón Basin is also characterized by continuous subsidence, but rates strongly increased at the beginning of the Neogene. Despite a rapid Plio-Pleistocene deformation of the fold-and-thrust belt, the present-day temperature field is not disturbed in that area. The modelling results indicate a mean heat flow of 60 mW m^{-2} for the North Limón Basin and 41 mW m^{-2} for the South Limón Basin. These values are low compared with other back-arc basins. The lower values are attributed to the following effects: (1) underlying basaltic crust, (2) the lack of an initial rift phase, (3) the low extension rates, (4) absence of volcanic activity and (5) insulation effects of a thick sediment pile. The reasons for the locally lower heat flow in the southern sub-basin can be found in the low-angle subduction of the Cocos Ridge. Owing to the low subduction angle, the cool fore-arc mantle-wedge below the island-arc is pushed backwards increasing the cooled area.

INTRODUCTION

The thermal history of sedimentary basins is one of the most important factors for the hydrocarbon potential and also influences the fluid flow and sediment compaction in a basin as well as the physical properties of fluids and sediments (e.g. Lerche *et al.*, 1984; Gosnold & Fischer, 1986; McCulloh & Naeser, 1989; Yalcin, 1991). In the last 20 years, basin modelling has become a widely accepted tool for reconstructing the burial history and related temperature evolution of sedimentary basins (e.g. Mareschal, 1987; Jensen, 1997; Rodriguez & Littke, 2001). Modern software can be used for the simulation of fluid flow and the generation and expulsion of hydrocarbons within the basin (e.g. Welte & Yükler, 1981; Welte & Yalcin, 1987; Ungerer *et al.*, 1990; Zhou & Littke, 1999; Yahi *et al.*, 2001). Basin modelling is extensively used in the oil industry and has been applied to academic problems in the last decade (e.g. Petmecky *et al.*, 1999; Nöth *et al.*, 2001; Lutz *et al.*, 2004; Rodon & Littke, 2005).

In recent times, complex geological settings such as foreland basins and fold-and-thrust belts have become interesting exploration targets. The structural style and evolution of fold-and-thrust belts have been discussed by many authors (Boyer & Elliott, 1982; Davis *et al.*, 1983; Dahlen, 1984; Dahlen *et al.*, 1984; Vergés *et al.*, 1992; Price, 2001). Numerical modelling studies were carried out on the structural development (e.g. Burbridge & Braun, 2002) and on the temperature evolution of fold-and-thrust belts (Schneider, 2003). The effect of folding and thrusting on the thermal field and on the fluid flow in fold-and-thrust belts has received special emphasis (Wygrala *et al.*, 1990; Schmidt & Erdogan, 1993; Husson & Moretti, 2002). In general, folding and thrusting can be regarded as a competition between advection and conduction of heat. If advection is faster than conduction, the thermal field will

Correspondence: Christian Brandes, Institut für Geologie, Leibniz Universität Hannover, Callinstr, 30, 30167 Hannover, Germany. E-mail: brandes@geowi.uni-hannover.de

be disturbed. If the ratio between diffusion and advection velocities is ≤ 1, there is no distortion (Husson & Moretti, 2002). Whether the folding has an effect on the thermal field depends on the relationship between the wavelength and amplitude of the folds, as well as the velocity of folding and the thermal conductivity of the rocks (Sleep, 1979). In the case of large wavelengths, large amplitudes and high deformation rates, the isotherms will be folded with the bedding planes. Nevertheless, there are still many open questions especially with respect to a quantitative understanding of the balance between conductive and advective heat transport in compressive settings.

The Limón back-arc basin is a complex basin-system. An extensional back-arc area (the North Limón Basin) and a compressional retro-arc foreland basin (the South Limón Basin) can be observed side by side. Both sub-basins are very similar regarding the stratigraphy and lithology of their fill, but differ significantly in the structural style and basin morphology. The setting of the Limón Basin provides the opportunity to identify the controlling factors of arc-related sedimentary basins such as subsidence rates and deformation. Our modelling study focuses on reconstructing burial history and temperature evolution. By comparing the thermal evolution from both sub-basins, we evaluate the impact of folding on the evolution of the thermal field.

GEOLOGICAL SETTING

The geology of southern Central America has been discussed in many previous studies (Weyl, 1980; Astorga, 1988; Lundberg, 1991; Seyfried *et al.*, 1991; Winsemann & Seyfried, 1991; Weinberg, 1992; Winsemann, 1992; Amann, 1993; Krawinkel & Seyfried, 1994; von Huene & Flüh, 1994; Barboza *et al.*, 1995; Werner *et al.*, 1999; Krawinkel *et al.*, 2000; Abratis & Wörner, 2001; Gräfe *et al.*, 2002; Calvo, 2003; Krawinkel, 2003). Most of the recent work was carried out in the field of marine geology/marine geophysics (Ranero & von Huene, 2000; Ranero *et al.*, 2000a, b; Barckhausen *et al.*, 2003). Several publications focus on plate tectonic reconstructions (e.g. Pindell *et al.*, 1988; Ross & Scotese, 1988; Frisch *et al.*, 1992; Astorga, 1997; Maresch *et al.*, 2000; Meschede *et al.*, 2000). Other studies deal with the petroleum potential of Costa Rica (Sheehan *et al.*, 1990; Astorga *et al.*, 1991; Barboza *et al.*, 1997; Barrientos *et al.*, 1997; Petzet, 1998; Lutz, 2002; Lutz *et al.*, 2004).

Central America is characterized by the interaction of five lithospheric plates, including the oceanic Cocos, Nazca and Caribbean Plates and the continental North and South American Plates (Fig. 1a). The Cocos and Nazca Plates are subducting beneath the Caribbean Plate along the NW–SE-trending Central America trench. The present-day subduction velocity off Costa Rica, relative to the Caribbean Plate, is 8.5 cm year^{-1} (DeMets, 2001). The Cocos Plate is characterized by the large NE–SW-trending Cocos Ridge, an asesimic ridge, which is a more than 1000-km-long, 250–500-km-broad structure that rises 2000 m above the adjacent seafloor. It has been subducted beneath southern Costa Rica since at least 3.6 Ma (Collins *et al.*, 1995; Walther, 2003).

The Central American land-bridge is a complex assemblage of four crustal blocks. From SE-Guatemala to NW-Colombia the Maya, Chortis, Chorotega and Choco Blocks can be distinguished (Donnelly, 1989; Weinberg, 1992; Di Marco *et al.*, 1995; Campos, 2001) (Fig. 1a). The Maya and Chortis Blocks have a continental basement, whereas the Chorotega and Choco Blocks represent island-arc segments underlain by a Mesozoic oceanic crust (Escalante & Astorga, 1994). The Costa Rican part of the island-arc (Chorotega Block) can be subdivided into a northern and a southern arc segment (Seyfried *et al.*, 1991). The northern arc segment is bounded to the north by the Hess Escarpment and to the south by the Trans Isthmic Fault System (Fig. 1a). Both features are important tectonic elements. The Hess Escarpment is a NE–SW-trending bathymetric feature in the Caribbean Sea, separating the continental Chortis Block from the oceanic Colombia Basin (Krawinkel & Seyfried, 1994; Campos, 2001). In previous studies, the Hess Escarpment was interpreted to represent a late Mesozoic plate boundary, which acted as a strike–slip zone to compensate the movements between Chortis Block, Chorotega Block and the Caribbean Plate (Krawinkel, 2003). The Trans Isthmic Fault System is an E–W-trending active lineament. It mainly shows sinistral movements and links a transtensional graben structure of southeastern Nicoya with the Limón Thrust Belt (Krawinkel & Seyfried, 1994). The southern Costa Rican arc segment is located south of the Trans Isthmic Fault System and belongs to the Panama Microplate. An important structural element of the southern arc segment is the North Panama Deformed Belt, dominating northern Panama. The development of this fold-and-thrust belt has largely been controlled by the collision of Panama with South America since Miocene times, the forward movements of the Nazca Plate and the oroclinal bending of the arc (Kolarsky *et al.*, 1995; Silver *et al.*, 1995).

In general, the evolution of most of the arc-related sedimentary basins started in Cretaceous times in response to

Fig. 1. (a) Tectonic map of Costa Rica. The Limón Basin extends along the Caribbean coast. The basin is separated into a northern and a southern sub-basin by the E–W-trending Trans Isthmic Fault System (modified after Ross & Scotese, 1988; Donnelly, 1989; Barboza *et al.*, 1995; Meschede & Frisch, 1998; Campos, 2001). The North Limón Basin is an extensional back-arc basin; the South Limón Basin is a compressional retro-arc foreland basin. Both sub-basins are very similar regarding the stratigraphy and lithology of their fill, but differ significantly in the structural style and basin morphology. (b) SW–NE-trending section of the offshore North Limón Basin. This section shows characteristics of passive margins. The large listric normal faults give evidence for a Plio-Pleistocene extensional phase. (c) SW–NE-trending cross-section from the offshore South Limón Basin, showing the structure of the Limón fold-and-thrust belt.

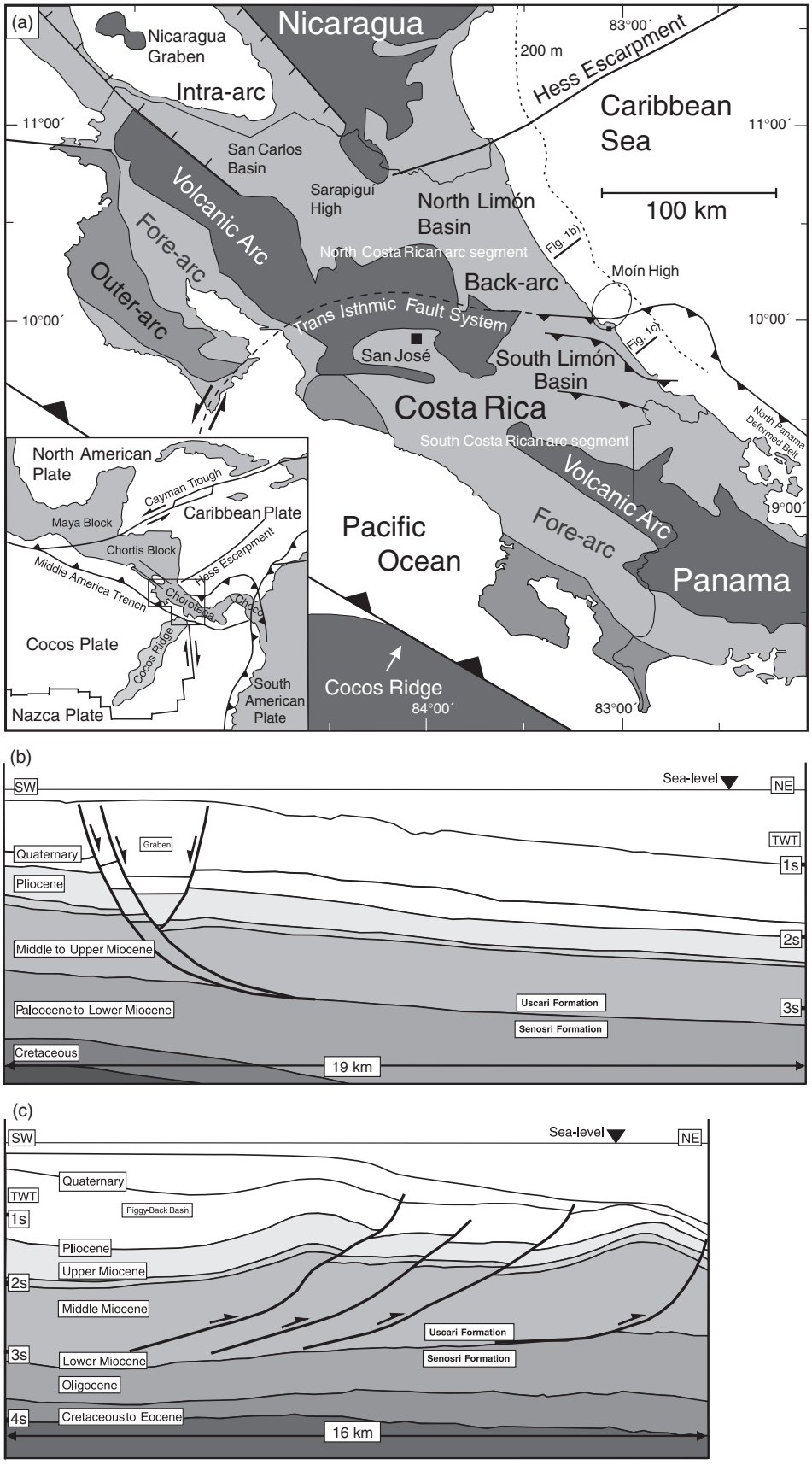
(a)
Nicaragua
Nicaragua Graben
Intra-arc
San Carlos Basin
Volcanic Arc
Fore-arc
Outer-arc
Sarapiquí High
North Limón Basin
North Costa Rican arc segment
Back-arc
Trans Isthmic Fault System
San José
South Limón Basin
Costa Rica
South Costa Rican arc segment
Volcanic Arc
Fore-arc
Panama
Pacific Ocean
Cocos Ridge
Hess Escarpment
Caribbean Sea
200 m
100 km
Moín High
Fig. 1b
Fig. 1c
North Panama Deformed Belt
83°00´
11°00´
10°00´
9°00´
84°00´
North American Plate
Cayman Trough
Caribbean Plate
Maya Block
Chortis Block
Middle America Trench
Chorotega
Choco
Cocos Plate
Cocos Ridge
South American Plate
Nazca Plate
(b)
SW
NE
Sea-level
TWT
1s
2s
3s
Quaternary
Graben
Pliocene
Middle to Upper Miocene
Paleocene to Lower Miocene
Uscari Formation
Senosri Formation
Cretaceous
19 km
(c)
SW
NE
Sea-level
TWT
1s
2s
3s
4s
Quaternary
Piggy-Back Basin
Pliocene
Upper Miocene
Middle Miocene
Lower Miocene
Oligocene
Cretaceous to Eocene
Uscari Formation
Senosri Formation
16 km

the onset of subduction of the Farallón Plate beneath the Caribbean Plate. The evolving tholeiitic island-arc shed large amounts of volcaniclastic material into the adjacent sedimentary basins (Seyfried *et al.*, 1991).

The Limón back-arc basin belongs to the southern Central American arc-trench system and is situated beneath the present-day coastal plain and continental shelf of eastern Costa Rica (Fig. 1a). The northern boundary is the Hess Escarpment. To the west and to the south, the basin is fronted by the volcanic arc. The eastward extent is defined by the 200 m bathymetric contour line of the Caribbean Sea and by the extent of the Limón fold-and-thrust belt, respectively. The fill of the Limón Basin consists of Late Cretaceous to Pleistocene deep-marine to continental volcaniclastic rocks (Sheehan *et al.*, 1990; Coates *et al.*, 1992, 2003; Amann, 1993; Bottazzi *et al.*, 1994; Fernandez *et al.*, 1994; McNeill *et al.*, 2000; Campos, 2001; Mende, 2001) (Fig. 2). Deposition of carbonates occurred during the Late Cretaceous, Eocene and Oligocene.

The North Limón Basin belongs to the North Costa Rican arc segment and is undeformed. Outcrops are rare and most information comes from two-dimensional (2D) seismic reflection lines (Fig. 1b) and some wells. Aeromagnetic data imply that the central basin is more than 7000 m deep (Barboza *et al.*, 1997). To the NW, the Sarapiquí High separates the North Limón Basin from the San Carlos intra-arc basin (Barrientos *et al.*, 1997). Some authors, however, integrate the San Carlos Basin into the North Limón Basin (Sheehan *et al.*, 1990). The basin is still subsiding (Mende, 2001).

The South Limón Basin belongs to the South Costa Rican arc segment and contains approximately 6–8 km of sedimentary rocks. The basin-fill has been deformed by NE-directed folding and thrusting (Fig. 1c). The resulting fold-and-thrust belt is referred to as the Limón fold-and-thrust belt in this study. All stratigraphic information for the South Limón Basin is based on onshore outcrops and well data (Amann, 1993; Bottazzi *et al.*, 1994; Fernandez *et al.*, 1994). The oldest sediments are ~1280-m-thick pelagic limestones and intercalated volcaniclastic rocks of Late Campanian to Maastrichtian age (Changuinola Formation, Fig. 2). The overlying Tuís Formation consists of ~3000 m of Palaeocene to Lower Eocene coarse-grained volcaniclastic turbidites, debris-flow deposits, lava-flows and tuffs, representing a prograding deep-water apron-system (Mende, 2001). An early compressional phase affected the island-arc during Eocene to Oligocene times and led to the formation of significant topographic relief, as implied by the simultaneous deposition of 150–200-m-thick shallow-water limestones of the Las Animas Formation on local structural highs (Amann, 1993; Mende, 2001), and 700–900-m-thick hemipelagic mudstones, calcareous turbidites and carbonate debris-flow deposits of the Senosri Formation in adjacent basinal areas (Mende, 2001). On top of these carbonates ~2000-m-thick shallow-water volcaniclastic sediments of the Upper Oligocene to Upper Miocene Uscari Formation were deposited (Amann, 1993; Mende, 2001). The Uscari

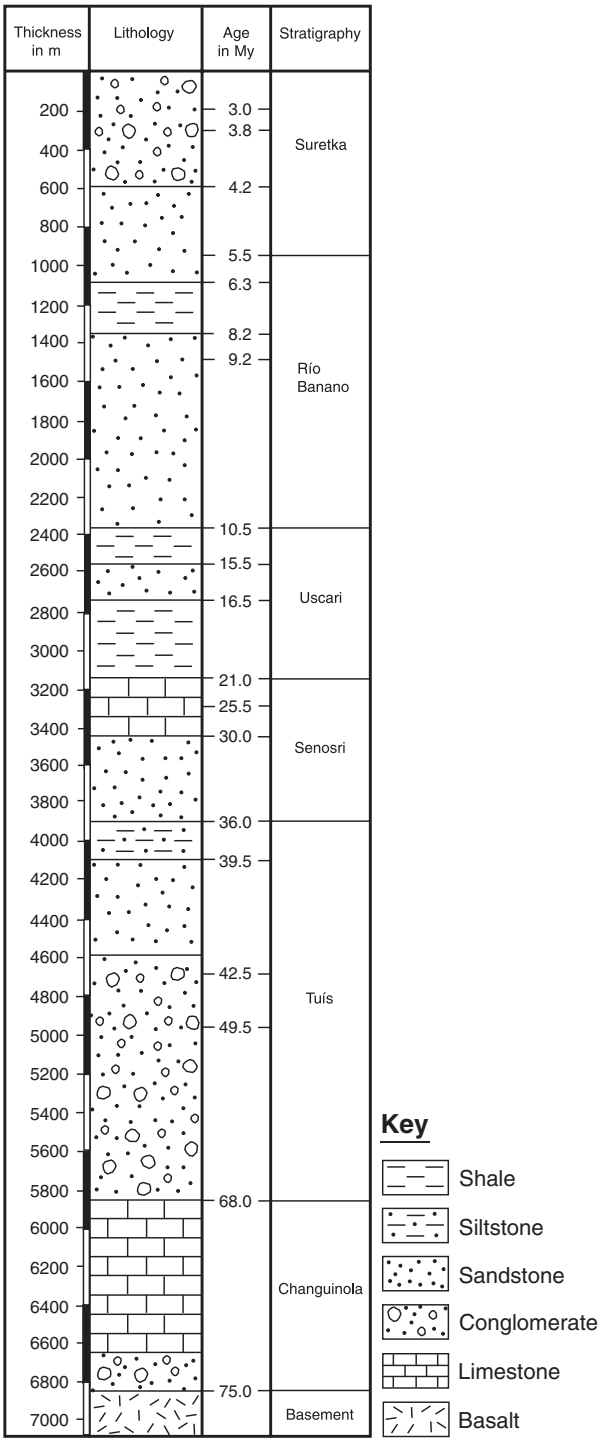

Fig. 2. Stratigraphy of the South Limón Basin (modified after Campos, 2001).

Formation is overlain by the shallow-water limestones and volcaniclastic rocks of the 400–1800-m-thick Río Banano Formation (Amann, 1993; Bottazzi *et al.*, 1994; Mende, 2001). The subduction of the Cocos Ridge beneath the island-arc began during the Late Miocene to Early Pliocene (Collins *et al.*, 1995; Abratis & Wörner, 2001). This led to increased NE-directed folding and thrusting and the development of small intramontane piggy-back basins. Subsequently, shallow-marine and continental

rocks of the Plio-Pleistocene Suretka Formation were deposited (Amann, 1993; Bottazzi *et al*., 1994; Mende, 2001).

DATABASE AND METHODS

The database includes a grid of 2D seismic reflection lines aquired during onshore and offshore campaigns in the 1970s and 1980s by the national oil company of Costa Rica (RECOPE) (Fig. 3). The grid consists of NE–SW- and NW–SE-directed seismic lines. Our interpretation of the seismic sections was performed with the software package Kingdom Suite©. Seismic sections are one of the building blocks of the conceptual model for the basin simulation. Therefore, the interpretation focused on the reconstruction of the basin-fill architecture. Stratigraphic and lithologic control for the interpretation is derived from one onshore well for each sub-basin. These wells were drilled by RECOPE in the late 1980s as stratigraphic tests in each sub-basin (Well #1 and #2). Well #1 is the key well for the interpretation of the seismic section from the North Limón Basin. It penetrates Pleistocene to Eocene sandstones, shales and limestones. Well #2 is the key well for the interpretation of the seismic sections of the South Limón Basin. It penetrates Pleistocene to Miocene sandstones, shales and limestones. The Cretaceous to Palaeocene portions of the basin-fill that were not drilled were interpreted on the basis of published outcrop data (Astorga *et al*., 1991; Campos, 2001; Mende, 2001). Depth conversion was performed for the two modelled sections and for the sections, which were used for the reconstruction of balanced cross-sections. The depth conversion was performed on the basis of interval velocities. Basin modelling focused on burial history and temperature evolution, carried out with the software PetroMod® 2D for one cross-section of each sub-basin. The modelled cross-sections are indicated by the bold lines in Fig. 3. We chose these lines because they cover a large part of each sub-basin and the nearby well provides the input and calibration data for the simulations. In addition, a 1D simulation was

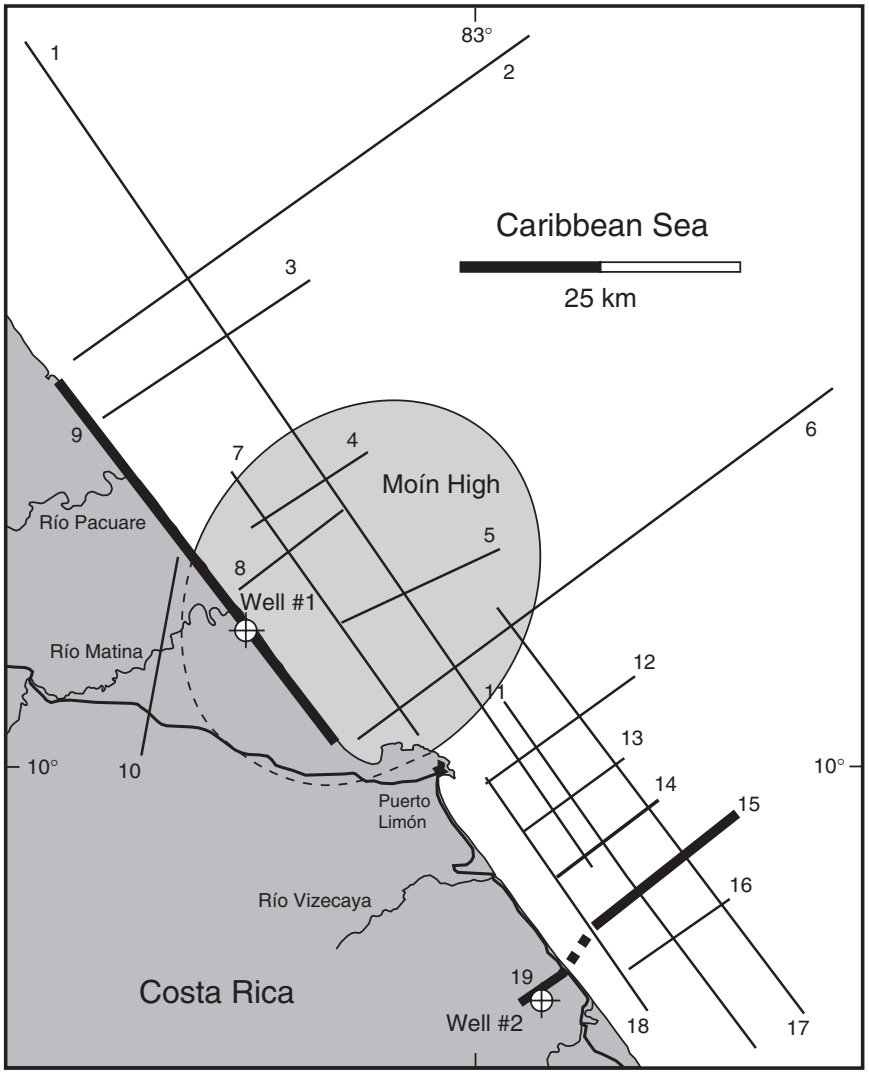

Fig. 3. Location map of the seismic lines and the two key wells. The key wells (Well #1 and #2) provide the calibration data for the simulation. The bold seismic lines indicate the foundation for the basin modelling.

carried out for each sub-basin based on well data to check the results derived from the 2D simulations. All numerical models were calibrated with vitrinite reflectance data and bottom-hole temperatures. These data are unpublished and were provided by the Ministry of Environment and Energy (MINAE). Additional input data like the variations of waterdepth over time were also taken from these unpublished reports. For the structurally complex South Limón Basin, balanced cross-sections have been reconstructed to estimate the amount of horizontal shortening.

SEISMIC INTERPRETATION AND BASIN-FILL ARCHITECTURE OF THE LIMÓN BASIN

The North Limón Basin is characterized by continuous depositional units, which can be laterally traced for several tens of kilometres on the NW–SE-directed seismic lines. The NE–SW-directed lines, which run perpendicular to the slope, display a wedge-shaped geometry of the accumulated sediments (Brandes *et al.*, 2007a). The sedimentary units display a pronounced seaward dip with the highest sediment thickness close to the present-day coastline (Fig. 1b). This depositional style is characteristic of passive margin settings in the circum Atlantic area (e.g. Hutchinson *et al.*, 1982; Bond *et al.*, 1995). Large listric normal faults can be observed in the shelf area (Fig. 1b). These faults trend NW–SE and belong to small graben structures. The major normal faults of the graben structures sole into a common detachment (Brandes *et al.*, 2007b). Borehole data indicate that the position of the detachment is probably controlled by the lithological change from shale of the Uscari Formation to limestone of the Senosri Formation (Fig. 1b).

An antiformal structure, referred to as Moín High, separates the North and South Limón Basin and was interpreted to represent a basement high in previous studies (Sheehan *et al.*, 1990; Barboza *et al.*, 1997). The Moín High has a convex, mound-like shape (Fig. 4). The internal structure is difficult to image with seismic methods. A strong reflector envelopes the Moín High and separates it from the surrounding sedimentary rocks. Below the reflector the Moín High is weakly layered (Brandes *et al.*, in press). On the northern flank of the structure a more continuous reflector pattern can be observed. The Moín High is draped with Middle Miocene and younger deposits. Upper Eocene to Lower Miocene units display an onlap pattern or pinch out against the Moín High. Well #1 was drilled on the northern flank of the structure and terminates in Middle Eocene carbonates. These rocks are directly overlain by Early Miocene shales. Upper Eocene and Oligocene deposits are absent at the drill site. The wedging of reflector packages against the Moín High implies that these units are present in the deeper parts of the basin. Therefore, the unconformity is interpreted as a local feature, limited to the flank of the structure. From this data set, the Moín High is interpreted as an anticline, which evolved between Middle Eocene and Early Miocene times (Brandes *et al.*, in press).

The South Limón Basin is characterized by the Limón fold-and-thrust belt (Fig. 1c). The seismic grid is denser in the South Limón Basin and allows a detailed assessment of the structural style of the deformed belt. The best insight into the architecture of the fold-and-thrust belt is provided by the NE–SW-directed seismic lines. These lines run roughly parallel to the direction of maximum compression. The offshore part of the Limón fold-and-thrust belt is characterized by concentric or asymmetric hangingwall anticlines and large southwestward-dipping listric or planar thrusts (Brandes *et al.*, in press). The offset at the thrust faults ranges between 50 m and 1 km. All thrusts sole into a subhorizontal detachment. Below the detachment no significant deformation can be observed. The detachment lies within the sedimentary rocks, resulting in a thin-skinned fold-and-thrust belt. Lithological logs derived from Well #2 indicate that the position of the detachment occurred at the change from shale of the Uscari Formation to limestone of the Senosri Formation (Brandes *et al.*, in press). Therefore, the rheologic contrast from shale to limestone probably controlled the position of the detachment. Remarkable features associated with the fold-belt are small and lenticular piggy-back basins. These basins contain some of the youngest sediments of the South Limón Basin.

Deformation phases of the Limón Basin

The Central American island-arc was affected by three major deformation phases since the Cretaceous (Seyfried *et al.*, 1991; Krawinkel *et al.*, 2000). Based on our seismic data, two different deformation phases could be reconstructed in the Limón Basin since the Palaeocene. The Moín High is a key element in the structural analysis. Onlap geometries in the vicinity of the structure imply that a first compressional phase affected that area between the Middle Eocene and the Early Miocene (Brandes *et al.*, 2007a). This phase caused the initial uplift of the Moín High. Upper Eocene and Oligocene deposits are absent on the northern flank of the Moín High. Early to Middle Miocene strata show a distinct onlap against the structure or pinch out. A small graben on the top of the Moín High is interpreted as a crestal collapse structure that is related to the formation of the anticline. Based on the sediment thickness distribution across the Moín High, it can be deduced that a second but weaker phase of uplift occurred between the late Middle Miocene and the Pliocene (Brandes *et al.*, 2007a). Since then, the Moín High was draped with sediments. No further vertical movements are documented. North of the Moín High the Limón Basin shows large listric NW–SE-trending normal faults, which can be attributed to a Pleistocene extensional phase (Brandes *et al.*, 2007a).

For the South Limón Basin, thickness variations across the thrust faults provide evidence of the timing of deformation-improving estimates of the temporal evolution of

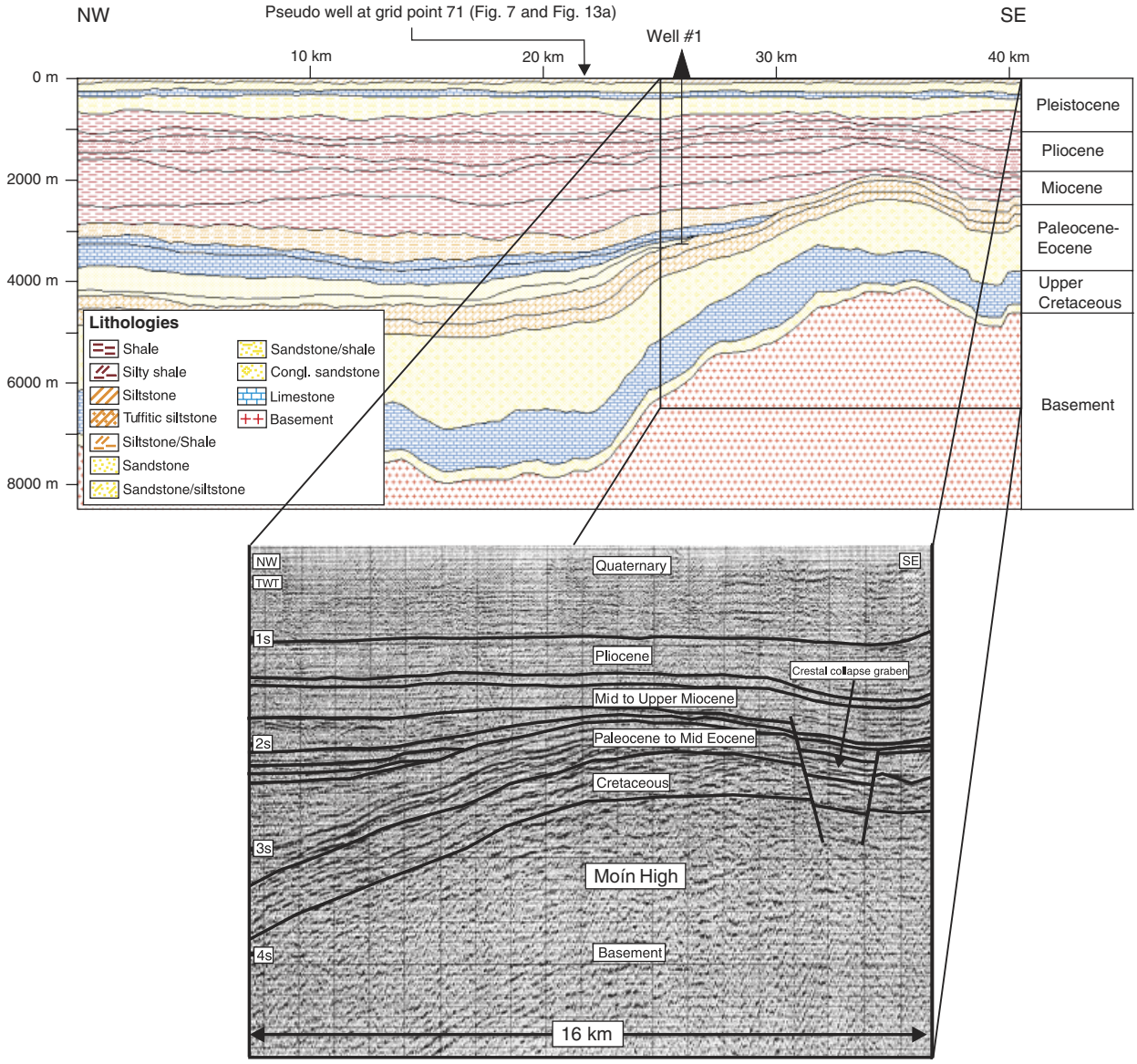

Fig. 4. Conceptual model for the North Limón Basin. The section runs parallel to the coastline and is characterized by continuous depositional units with a constant thickness. The close-up shows the seismic data of the convex Moín High. The graben on top of the Moín High is interpreted as a crestal collapse structure that evolved during the rise of the anticline.

the fold-and-thrust belt. The offshore part of the South Limón Basin was affected by compression since the Pliocene. However, most of the deformation occurred during the Pleistocene (Brandes *et al.*, in press).

BASIN MODELLING, CONCEPTUAL MODEL AND MODELLING RESULTS

The 2D thermal simulations are based on one seismic line from each sub-basin. Lithologic information and calibration parameters are derived from key wells (Well #1 and #2), located on or close to each of the seismic lines. Additional data from unpublished exploration reports were integrated. The locations of the modelled sections are shown in Fig. 3. Table 1 shows the physical properties of the rocks that were used in the simulation.

Basin modelling

The basin modelling part of this project was carried out with the software PetroMod® 1D/2D, which was developed by IES GmbH, Germany. PetroMod® allows us to study the burial history and temperature evolution of a sedimentary basin and the related generation and migration of hydrocarbons. It is a dynamic forward simulation, based on the finite element method. The finite element grid used for the 2D simulations has rectangular cells defined by vertical grid lines and horizontal event lines. The horizontal event lines are defined by time lines derived from the seismic interpretation. The vertical grid lines are placed equidistantly along the section to generate a mesh. During the simulation, the finite element grid is fixed to the objects and subsides with the layers (Friberg, 2001). A basin modelling study with PetroMod® follows a standard workflow.

Table 1. Physical properties of the rocks that were used in the simulation

Lithology	Density (kg m^{-3})	Porosity (%)	Compressibility (10^{-7} kPa)		Thermal conductivity (W m K^{-1})		Heat capacity (kJ kg K^{-1})	
			Max	Min	20 °C	100 °C	20 °C	100 °C
Shale	2680	65	60 000	10	1.98	1.91	0.213	0.258
Silty shale	2677	62	25 000	10	2.05	1.94	0.21	0.254
Shale/siltstone	2674	59	13 000	10	2.09	1.97	0.207	0.251
Shale/limestone	2695	53	1500	20	2.39	2.24	0.208	0.246
Siltstone	2672	56	8000	10	2.14	2.03	0.201	0.242
Siltstone/shale	2674	59	13 000	10	2.09	1.97	0.207	0.251
Tuffitc siltstone	2666	56	9000	10	2.27	2.13	0.201	0.242
Sandstone	2660	42	500	10	3.12	2.64	0.178	0.209
Conglomeratic sandstone	2663	35	330	10	2.93	2.63	0.184	0.217
Sandstone/siltstone	2665	50	1900	10	2.59	2.31	0.192	0.229
Limestone	2710	24	150	10	2.83	2.56	0.195	0.223
Shaly limestone	2700	37	550	10	2.51	2.31	0.203	0.237
Marl	2687	47	940	10	2.23	2.11	0.208	0.248
Basement	2750	5	2	1	2.72	2.35	0.188	0.223

At first a conceptual model must be created, which is based on the results of basin analysis. The conceptual model is the description of the geologic evolution of a basin (Poelchau *et al*., 1997). For such a conceptual model, the complex real system must be simplified and reduced to a few fundamental parameters (Welte & Yükler, 1981). The conceptual model is designed on the basis of the basin-fill architecture. Then the depositional history of the basin is divided into distinct events. Each event can represent a phase of deposition, non-deposition or erosion. It is necessary to reconstruct the complete evolution of a sedimentary basin. Therefore episodes of non-sedimentation or even erosion must be quantified (Poelchau *et al*., 1997). Absolute ages and, in a second step, lithologies must be assigned to each event. The absolute age is important to reconstruct the temporal evolution. The lithology determines the thermal conductivity of the basin-fill and the behaviour during compaction.

The next step is to define a set of boundary conditions that describe the state of the model at its boundaries. The boundary condition can be constant or variable during the simulation, depending on the requirements of the study. The most important boundary conditions are the basal heat flow and the temperature at the earth surface (Yalcin, 1991; Yalcin *et al*., 1997). The basal heat flow is chosen according to the geological setting. The surface temperature is determined by the geographic position of the basin and by the water depth. These parameters are not stable and change during the evolution of the basin (Poelchau *et al*., 1997). Therefore, these changes must also be considered in the simulation. PetroMod® has a tool to reconstruct the surface temperature based on palaeolatitude and palaeo-water depth. Plate drift and related climatic changes are incorporated into the simulation. After the simulation, the resulting output must be compared with the real system in order to calibrate the model. The most important calibration parameters are vitrinite reflectance values and present-day temperature data. Both parameters are derived from wells close to the modelled section. Vitrinite reflectance is an indicator of the maturity of organic matter. It can be used for the determination of the palaeoheat flux and to optimize the thermal history models (e.g. Lerche *et al*., 1984; Durand *et al*., 1986). With increasing maturity of the organic material, the reflectivity of the vitrinites also increases. The maturation of vitrinites can be described with reaction kinetics (Larter, 1989; Sweeney & Burnham, 1990). In this study, we used the widely accepted approach of Sweeney & Burnham (1990), which is based on the Arrhenius equation. It describes the maturation of vitrinites with increasing temperature, considering the loss of water, carbon dioxide and hydrocarbons. The rate of this reaction is a function of the activation energy and the frequency factor. The advantage of the kinetic approach of Sweeney & Burnham (1990) is its wide range. It can be used to calculate vitrinite reflectance values from 0.3 to 4.5%. During basin simulation, the program calculates the evolution of temperature and maturity parameters parallel to the evolution of the basin. After each run the simulated values can be compared with real data. If the simulated parameters fit to the measured ones, the simulation can be stopped. The calibrated model can now be used to predict further parameters, which were not directly measured in the real system. If the simulated and measured parameters diverge, the input must be adjusted until a sensible calibration is achieved.

In this study, two standard types of basin modelling techniques were applied. 1D basin modelling is based on well data. 2D basin modelling is performed for one cross-section of each sub-basin.

1D basin modelling

The 1D basin simulations were used to reconstruct the burial history and temperature evolution for a single point

in the basin. Input data for 1D modelling are derived from the key wells. As described above, the most important parameters are the age and thickness of the sediments as well as their lithologies. Boundary conditions for the simulation are the temperature at the base and at the surface of the model.

2D basin modelling

The 2D simulations of this study are based on seismic sections. The basin-fill architecture is integrated into the simulation. Before basin modelling the seismic lines were interpreted. Based on the key wells, which were tied to the seismic lines, the whole section was subdivided into as many layers as possible. The geometry and arrangement of the depositional units were transferred into a conceptual model. The lithology for each layer was derived from the key wells or published outcrop data. PetroMod® has a set of standard lithologies. Each lithology is characterized by several physical parameters (Table 1). Based on the description of the rocks, we chose the appropriate lithology in the modelling software. Again, the boundary conditions for the simulation are the temperature at the base and at the top of the model. Because of the integration of the basin-fill architecture, the 2D simulation allows us to reconstruct the basin evolution in a more realistic way. For example the lateral variations of the thermal field can be derived.

There is a difference in the input parameters between the 1D and 2D simulations in this study. Owing to well control in the upper parts of the stratigraphic sequence, the 1D models were split into more events. Therefore, the temporal and lithological resolution is higher. It was not possible to have similar detailed 2D models, because many of the lithologic intervals were below the resolution of the seismic sections. For the 2D models several intervals had to be merged. To avoid mistakes due to the simplifications, we used the 1D simulations to check the results of the 2D simulations. The heat flow derived from the 2D simulations is 3–4 $mW m^{-2}$ higher than the values derived from the 1D simulations. This difference in the results is regarded as insignificant.

The PetroMod® version used in this study is not able to simulate horizontal shortening. Therefore, folding of the strata was modelled as differential burial. The beds on the limbs of the anticlines were buried faster than the material on the crest of the anticlines. This approach also generates a realistic geometry of the basin-fill for each time step and allows a reasonable simulation of the thermal field.

North Limón Basin

Conceptual model

The cross-section for the 2D simulation is based on a NW–SE-trending onshore seismic line. The line is 40 km long and runs parallel to the coastline north of Puerto Limón (Fig. 3). We chose this section because it is one of the longest seismic sections from the North Limón Basin and a well (Well #1) is located on the seismic line that provides lithologic information for the conceptual model and the calibration parameters for the simulation. The section covers the southern part of the North Limón Basin and the top and the northwestern flank of the adjacent Moín High (Fig. 4). In the central part of the section the basin reaches a thickness of approximately 8000 m. Well #1 was drilled onshore north of Puerto Limón on the northern flank of the Moín High close to the present-day coastline. It penetrates Pleistocene to Middle Eocene sandstone, shale and limestone. The terminal depth is 3356 m. At a depth of 2910 m, Middle Eocene limestone is directly overlain by Early Miocene limestone. Upper Eocene and Oligocene deposits are missing. This unconformity is interpreted as a local feature, which resulted from vertical movements of the Moín High. The amount of vertical uplift is difficult to quantify, because it is not clear whether the Upper Eocene and Oligocene sediments were eroded or whether they were never deposited on the Moín High. The conceptual model for the 2D simulation consists of 21 layers (Table 2). The layers are based on well data and the seismic interpretation. The finite element mesh has 132 vertical grid lines.

The initial phase of evolution of the North Limón Basin started in Campanian time, with the deposition of *ca*. 300 m of conglomeratic sandstones, followed by *ca*. 1000 m of pelagic carbonates (Campos, 2001). The seismic interpretation shows that these sediments were deposited with a relatively constant thickness along the modelled section. The Palaeocene–Early Eocene period is characterized by conglomeratic sandstones that represent a deep-water slope-apron system (Mende, 2001). The water depth decreases from 2000 m (Campanian) to 150 m (Early Eocene) (MINAE, unpublished report). During the Early Eocene the evolution of the Moín High started. From the seismic line it can be determined that Early Eocene and Middle Eocene sediments were deposited on the Moín High with reduced thickness, compared with the deeper parts of the basin. Close to the northwestern margin of the Moín High, a small depocentre evolved, where sediments accumulated with slightly greater thicknesses than further to the northwest. Late Eocene to Early Middle Miocene units show an onlap against the Moín High. The period Eocene–Oligocene is characterized by a relatively shallow water depth of 200 m (MINAE, unpublished report). During the Miocene there was still tectonic activity at the Moín area. Middle to Late Miocene rocks still have a reduced thickness on the Moín High compared with the deeper parts of the basin. During this period the water depth increased from 200 m (Late Oligocene) to 1000 m (Late Middle Miocene) (MINAE, unpublished report). Whereas the Late Oligocene–Early Miocene was characterized by carbonate deposition, the subsequent Middle Miocene–Early Pleistocene period was dominated by shale deposition (Mende, 2001). The seismic section gives evidence for an increased sediment thickness of the Pliocene units in the crestal collapse graben on top of the Moín High. We interpret this as an indicator for ongoing

Table 2. Stratigraphy and input parameters of the conceptual model of the North Limón Basin at grid point 31

North Limón Basin						
Event No.	Event name	Age at the base in Ma	Lithology	Thickness in m (at GP 31)	Water depth (m)	SWIT (°C)
21	Holocene	0.01	Siltstone	105	0	23.1
20	Late Late Pleistocene	0.45	Sandstone and Siltstone	154	100	21.1
19	Middle Late Pleistocene	0.66	Limestone	92	50	22.1
18	Early Late Pleistocene	1.3	Sandstone and Siltstone	448	200	20.1
17	Early Pleistocene	1.8	Shale	363	500	8.8
16	Late Pliocene	2.9	Shale	108	300	16.3
15	Early Pliocene	5.3	silty Shale	228	800	5
14	Late Miocene	7.4	Shale	327	800	5
13	Late Middle Miocene	12.5	Shale	511	1000	5
12	Middle Middle Miocene	18.0	Shale	551	200	21.1
11	Early Middle Miocene	20.4	Siltstone and Shale	417	700	6.0
10	Early Miocene	23.0	Limestone	127	500	10.4
9	Late Oligocene	28.4	Limestone	386	200	21.7
8	Early Oligocene	33.9	Sandstone	387	200	22.4
7	Late Eocene	37.2	Sandstone	187	200	23
6	Middle Eocene	41.4	tuffitic Siltstone	261	200	23.7
5	Early Eocene	48.6	tuffitic Siltstone	258	150	24.5
4	Paleocene	65.5	congl. Sandstone	1253	900	16.5
3	Campanian-Maastrichtian	79.9	Limestone	866	2000	14.9
2	Early Campanian	83.5	congl. Sandstone	215	2000	15.2
1	Basement	90	Basement	4500	2000	15.2

SWIT (sediment water interface temperature) is the upper boundary condition for the simulation.

tectonic activity. The Pleistocene shows very high sedimentation rates (*ca*. 1100 m sandstone, siltstone and limestone were deposited in 1.8 Ma). From the seismic line, it can be determined that the Pleistocene to Recent deposits display a constant thickness distribution across the section. There is no evidence for differential tectonic activity in the Moín area. The water depth decreased continuously from 800 m (Late Miocene) to 0 m (Holocene) (Campos, 2001).

Calibration

The simulation was calibrated with vitrinite reflectance data and bottom-hole temperatures (Fig. 5). The measured vitrinite trend has an anomalous shape and shows a kink at 1500 m. Below the kink the trend is relatively steep. The calibration was performed using the Easy%Ro approach of Sweeney & Burnham (1990). We carried out a minimum/maximum scenario with a heat flow range between 30 and 85 $mW m^{-2}$. The simulated vitrinite trend was adjusted to the vitrinite reflectance measurements from the lower part of the sequence (2200–2800 m). A best fit of measured and simulated vitrinite reflectance trends was achieved with a mean heat flow of 60 $mW m^{-2}$. From a 1D simulation a mean heat flow of 56 $mW m^{-2}$ was derived. This difference in the results between the 1D and 2D simulation is not significant. A calibration of the vitrinite reflectance values in the upper part of the sequence (500–2000 m) is also possible if a heat flow of 85 $mW m^{-2}$ is used. However, the data in the lower part of the sequence do not fit in this case. Furthermore, the recent bottom-hole temperatures are not met. Therefore, it is assumed that the first calibration (60 $mW m^{-2}$) is more realistic. At least two possibilities exist to explain the high vitrinite reflectance data for the sequence of 500–2000 m: the first possibility is convective heating by hot fluids. In our opinion, this can be ruled out due to the low permeability of the shales. The second possibility is the presence of resedimented vitrinite derived from erosion of older rocks, as has been described (e.g. Radke *et al*., 1997; Taylor *et al*., 1998). Clearly, geothermal gradients are never linear due to the different conductivities of the rocks and are also influenced by compaction (Yalcin *et al*., 1997).

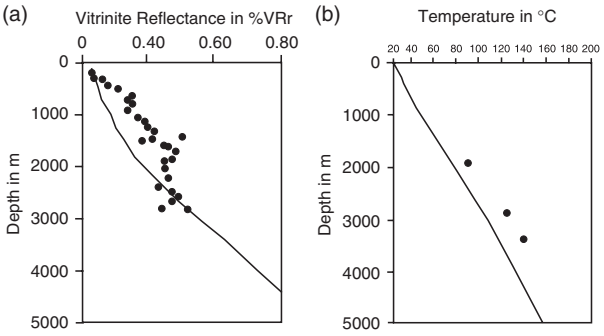

Fig. 5. Calibration for the North Limón Basin. (a) Vitrinite reflectance measurements from key Well #1 (black dots). The calibration was performed with the Easy%Ro approach of Sweeney & Burnham (1990). The simulated trend is given by the black line. (b) Bottom-hole temperatures from the key well (black dots). The simulated geothermal gradient is shown as a solid line.

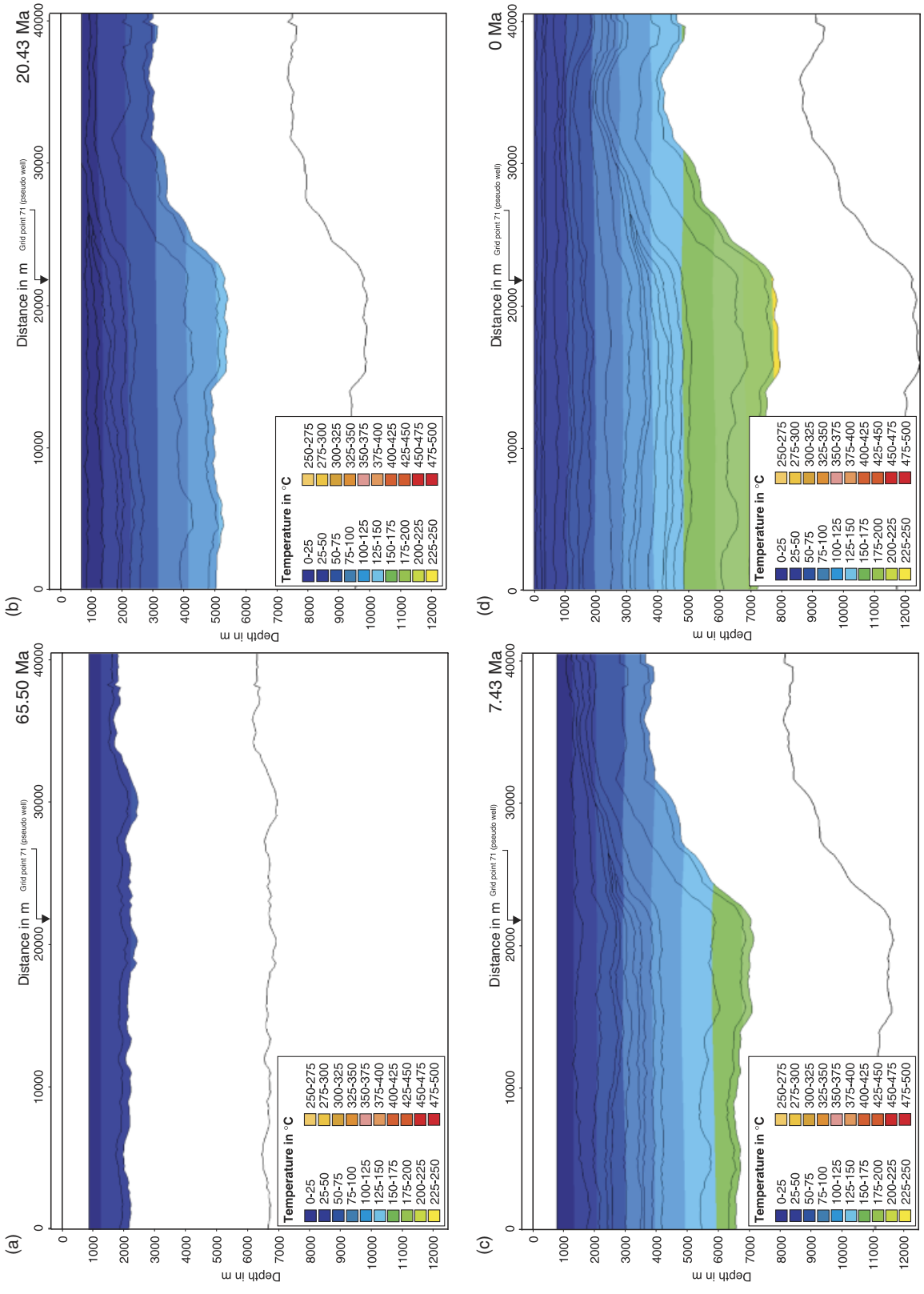

Fig. 6. Burial history of the North Limón Basin. The temperature evolution is shown with a colour overlay. The initial phase of basin evolution started in Cretaceous times (a). Figures (b) and (c) show Neogene time steps. The present-day temperature field is shown in (d).

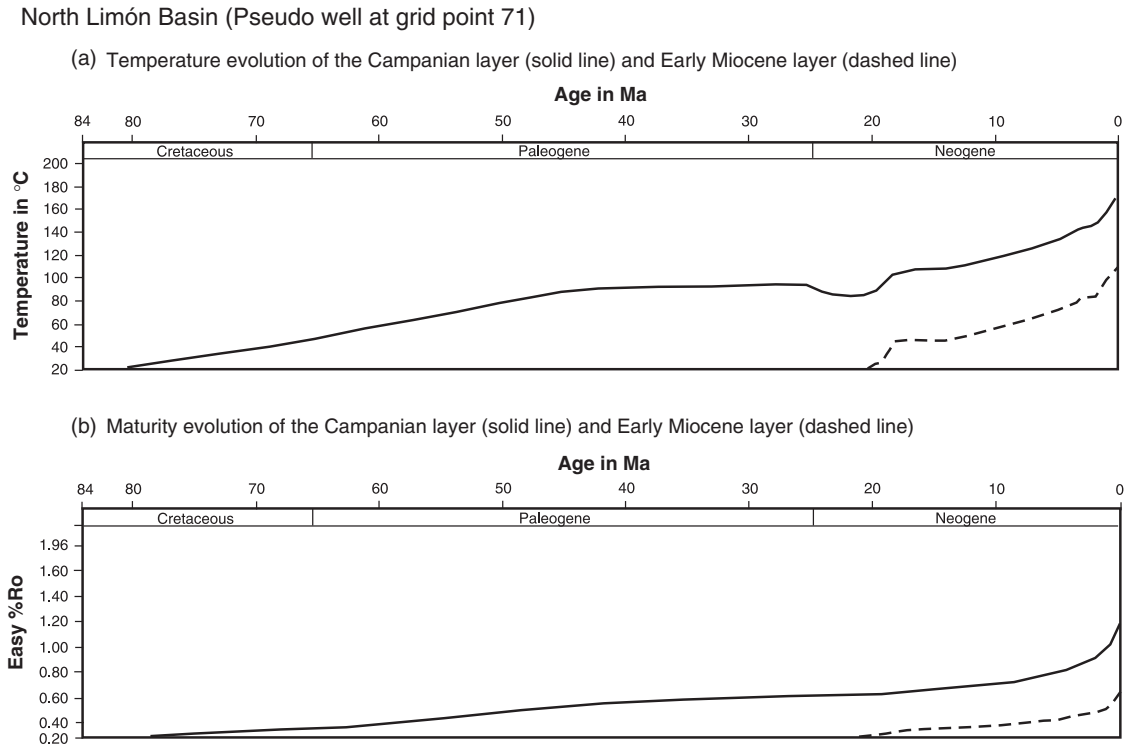

Fig. 7. Temperature and maturity evolution for the interval Campanian and Early Miocene in the North Limón Basin.

Modelling results

The most deeply buried rocks on the modelled section occur in the depocentre close to the northwestern margin of the Moín High. They reach a temperature of ~225–250 °C (Fig. 6). From a pseudo well at grid point 71, the temperature and maturity of the Campanian and Early Miocene layers were inferred. At that point the basin has a depth of 7800 m. The Campanian rocks have a recent temperature of ~160 °C and a maturity of ~1.20%VRr (Fig. 7a). For the Early Miocene rocks a recent temperature of ~100 °C and a maturity of ~0.60%VRr were derived (Fig. 7b). The simulation reveals that the evolution of the Moín High has no significant effect on the thermal field. The present-day temperature field is characterized by almost surface-parallel isotherms. Only a minor upwarp of the isotherms can be observed in the area of the Moín High. This indicates that the uplift of the Moín High was too slow for the temperature field to be disturbed.

South Limón Basin

Reconstruction of balanced cross-sections

The construction of balanced cross-sections is a geometric method used to quantify the amount of shortening or extension of a deformed basin-fill and to reconstruct the initial geometry (e.g. Dahlstrom, 1969; DePaor, 1988). In this study, the technique was applied to the South Limón Basin (Limón fold-and-thrust belt) prior to basin modelling. The basic concept behind the construction of balanced sections is 'compatibility'. That is all body translations, rotations and strains developed in a deformed mass of rock are controlled by geometric laws. In addition, the rock mass is conserved during deformation (Ramsey & Huber, 1987). Several rules and methods have been proposed for the construction of balanced cross-sections. According to Wilkerson & Dicken (2001), a cross-section is a balanced cross-section if the following four criteria are met: (1) interpreted geometries must reflect natural stuctures for the area of interest; (2) the pre-deformational strata must appear reasonable once folds are unfolded and slip is removed on faults; (3) mass must be conserved between the deformed cross-section and the restored cross-section; and (4) a physically possible kinematic history must describe the development of the structures from the undeformed to deformed state. A very common redeformation technique is line-length balancing (e.g. Dennison & Woodward, 1963; Ramsey & Huber, 1987). Line-length balancing was performed for three depth-converted seismic sections from the South Limón Basin. On each section the pre-deformation length of several interpreted seismic reflectors at different depth levels was reconstructed. For the section that is used for basin modelling the results point to a relatively low shortening of 8% (Fig. 8). Overall, the thrusts have a small displacement. We interpret that the horizontal shortening was mainly compensated by the development of the anticlines through fault-propagation folding. These types of folds have been discussed in great detail by e.g. Suppe (1983), Suppe & Medwedeff (1990) and Mitra (1990). The results from the other sections imply that there are significant variations in the amount of shortening in the Limón

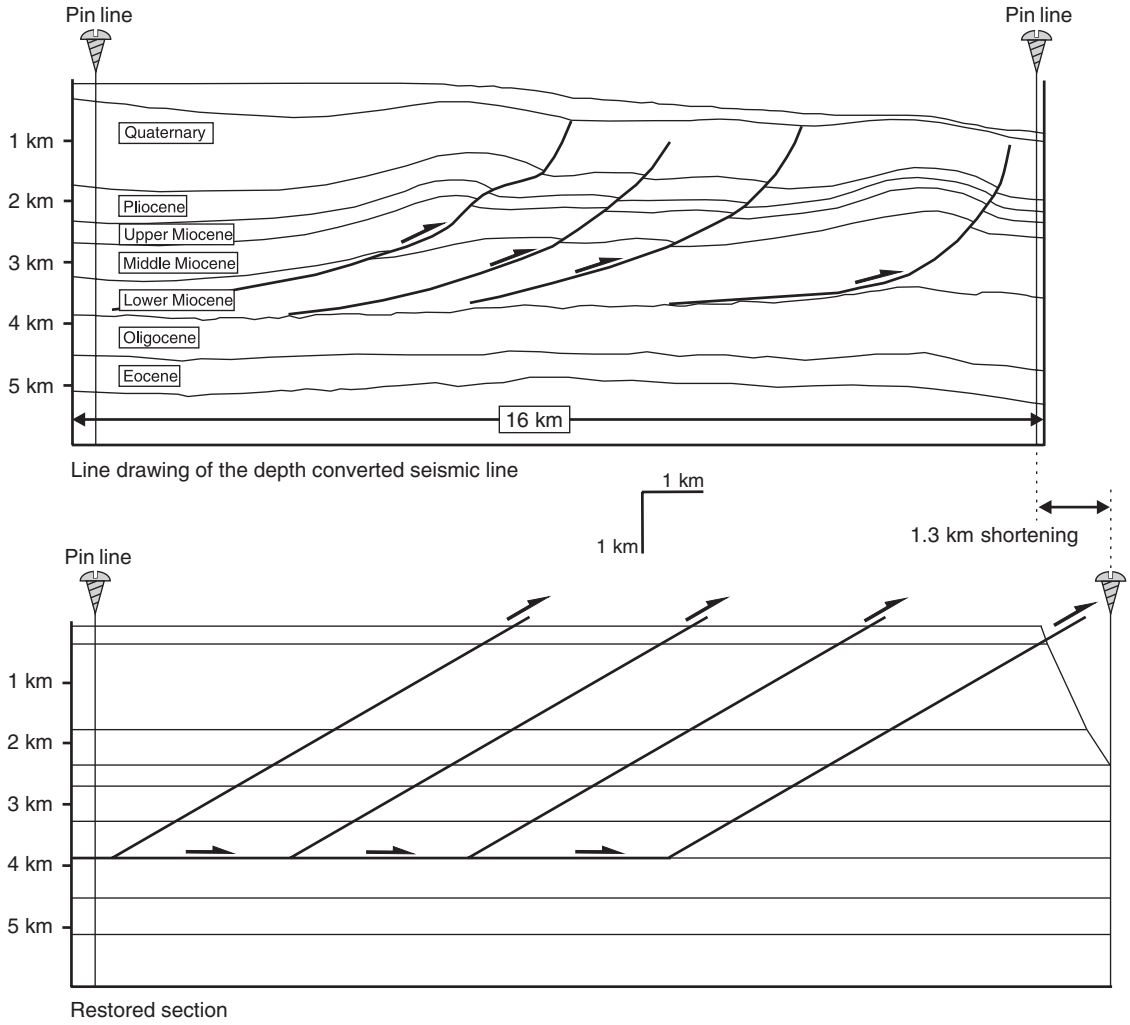

Fig. 8. Line-length balancing of a depth-converted seismic section from the South Limón Basin. For this section, which was also used for basin modelling, a shortening of 1.3 km (8%) is derived. The thrusts have a small displacement. Horizontal shortening was mainly compensated by the development of the anticlines throughout fault-propagation folding.

fold-and-thrust belt. In general, the shortening increases from the SE towards the NW. This observation can probably be explained by the interaction of the fold-and-thrust belt with the Moín High. The NW–SE-orientated seismic section shows that the southeastern flank of the Moín High is overthrust by the propagating deformed belt. The offsets along the thrust faults increase towards the Moín High. The Moín High acted as an obstacle for the fold-and-thrust belt. The propagation was limited and the movements were compensated with offsets along the thrusts (Brandes *et al*., 2007b).

Conceptual model

The section for the simulation of the South Limón Basin was created from two NE–SW-trending seismic lines (Fig. 3). A shorter onshore line and a longer offshore line were combined. An interpolation between the two lines was possible, based on seismic interpretation and the previous work of Bottazzi *et al*. (1994) and Fernandez *et al*. (1994). From SW towards NE, the section shows three pronounced anticline structures, which developed in the hangingwall of the main thrust faults (Fig. 9). The thrusts have more or less listric geometries and a very low displacement. Because of the low displacement the thrusts are not integrated into the conceptual model. From the structural restoration, it can be derived that most of the deformation along the section has been compensated by folding. In the northeastern-most part of the section, the deposits reach a thickness of approximately 8000 m (Fig. 9). We choose this section for the basin modelling, because it is the longest seismic line from the South Limón Basin that runs parallel to the direction of maximum compression. In addition, Well #2, a key well in the South Limón Basin is very close to this section. The well penetrates Pleistocene to Lower Miocene sandstones, shales and limestones. The terminal depth is 4202 m. The well data are used for the conceptual model and for calibrating the simulation. The conceptual model (Fig. 9) consists of 17 layers (Table 3). These layers were defined on the basis of the seismic interpretation and data derived from Well 1. Altogether,

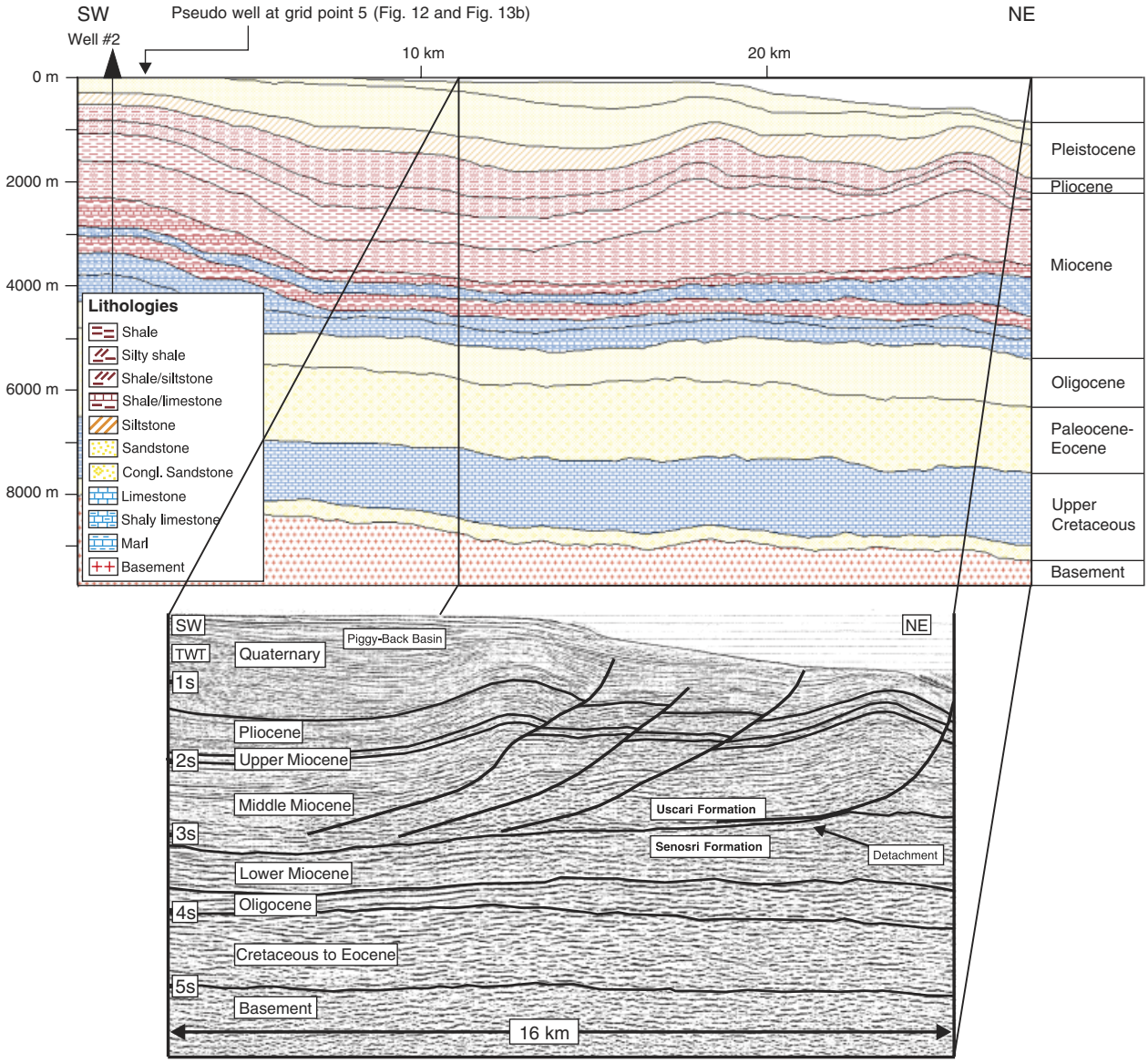

Fig. 9. Conceptual model for the South Limón Basin. The well shown on the section is Well #2. Middle Miocene to Pleistocene rocks are part of the thin-skinned Limón fold-and-thrust belt. The enlargement of the seismic line shows the offshore part of the fold-and-thrust belt. The thrusts are not integrated into the conceptual model because of the low displacement.

148 vertical grid lines were used to define the finite element mesh.

The evolution of the South Limón Basin started 83 Ma ago in the Campanian with the deposition of *ca*. 300 m of conglomeratic sandstone and ~1300 m of pelagic limestone (Mende, 2001). During the Palaeocene, ~1400 m of sandstone and conglomeratic sandstone were deposited (Campos, 2001). The seismic interpretation shows that Cretaceous and Palaeocene sediments have a constant thickness along the section. The Oligocene unit is still sandy, whereas the Early–Middle Miocene period is dominated by carbonate deposits (marl, limestone and shaly limestone) (Campos, 2001). The water depth decreases from 2000 m (Campanian) (Campos, 2001) to 200 m (Early Miocene) (MINAE, unpublished report). The Middle Miocene–Pliocene period is characterized by shaly and silty deposits. From the seismic line it can be seen that Early–Middle Miocene deposits have a constant thickness across the section. Deformation and evolution of the Limón fold-and-thrust belt started in the Pliocene (Brandes *et al.*, in press). During the Late Pliocene the first anticlines evolved. Most of the deformation occurred during the Pleistocene. Plio-Pleistocene sediments consist of sandstone, siltstone and shale and reach their greatest thickness of ~2000 m in the piggy-back basins. On the crest of the anticlines these deposits show a reduced thickness.

Calibration

The vitrinite trend from the South Limón Basin is quite steep and has a nearly linear shape (Fig. 10). The calibration was performed with the Easy%Ro approach (Sweeney & Burnham, 1990). To reconstruct the heat flow, a minimum/maximum scenario with a range of 25–65 mW m^{-2}

Table 3. Stratigraphy and input parameters of the conceptual model of the South Limón Basin at grid point 103

South Limón Basin						
Event No.	Event name	Age at the base (Ma)	Lithology	Thickness in m at (GP 103)	Water depth (m)	SWIT (°C)
17	Late Late Pleistocene	0.4	Sandstone	297	130	21.3
16	Eraly Late Pleistocene	1.2	Sandstone	493	130	21.3
15	Early Pleistocene	1.8	Siltstone	310	200	21.3
14	Pliocene	5.3	Shale and Siltsone	692	200	19.9
13	Late Miocene	7.4	Shale and Siltsone	223	350	15.2
12	Late Middle Miocene	11.8	Shale	480	500	8.9
11	Middle Middle Miocene	16.1	silty Shale	1128	400	11.7
10	Early Middle Miocene	20.4	Shale and Limestone	182	200	20.8
9	Late Early Miocene	20.8	shaly Limestone	270	200	20.2
8	Middle Early Miocene	21.5	Shale and Limestone	251	300	19.3
7	Early Early Miocene	22.3	Marl	136	300	18.4
6	Earliest Early Miocene	23.0	Marl	378	300	17.5
5	Oligocene	33.9	Sandstone	788	800	9.3
4	Paleocene-Eocene	65.5	congl. Sandstone	1426	900	14.5
3	Campanian-Maastrichtian	79.9	Limestone	1345	2000	14.9
2	Campanian	83.5	congl. Sandstone	290	2000	14.9
1	Basement	90	Basement	4500	2000	15

SWIT (sediment water interface temperature) is the upper boundary condition for the simulation.

was carried out. Similar to the North Limón Basin, the simulated vitrinite trend was adjusted to the vitrinite reflectance measurements from the lower part of the sequence (2900–4000 m). A best fit between measured and simulated trends was achieved with a mean heat flow of 41 mW m^{-2}. A mean heat flow of 38 mW m^{-2} was derived from a 1D simulation. The difference in the results is not significant. For the South Limón Basin it was also possible to calibrate with the vitrinite reflectance values of the upper part of the sequence (1000–2700 m) when if a heat flow of 58 mW m^{-2} is applied. However, the data in the lower part of the sequence do not fit in this case. The first calibration (41 mW m^{-2}) is therefore more realistic. Again different possibilities exist to explain the high vitrinite reflectance data for the upper part of the sequence. The first one is convective heating by circulating hot fluids. This can be ruled out due to the shaly nature of the sequence. The second possibility is the presence of resedimented vitrinite derived from erosion of older rocks as described by e.g. Radke *et al.* (1997), and Taylor *et al.* (1998). Clearly, geothermal gradients are also influenced by the conductivity of the rocks and are therefore not linear. From the simulations an average geothermal gradient for the upper crust of 2 °C 100 m^{-1} can be deduced, which is equal to the present-day geothermal gradient that was measured in the key well (Astorga *et al.*, 1991).

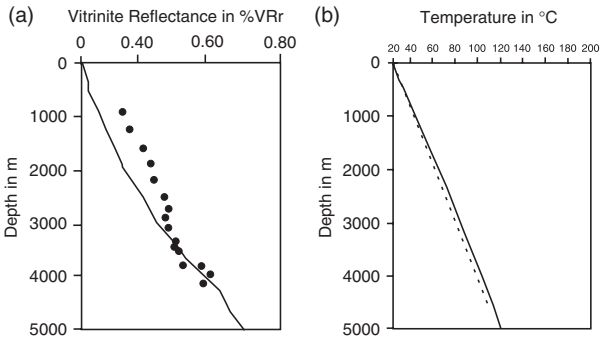

Fig. 10. Calibration for the South Limón Basin. (a) Vitrinite reflectance measurements from key Well #2 (black dosts). The calibration was performed with the Easy%Ro approach of Sweeney & Burnham (1990). The simulated trend is given by the black line. (b) The solid line shows the geothermal gradient derived from the simulation. The dashed line shows the observed gradient (2 °C 100 m^{-1}) in Well #2.

Modelling results

The most deeply buried rocks in the section reach a temperature of ~180–200 °C (Fig. 11). From a pseudo well at grid point 5, the temperature and maturity of the Campanian and Early Miocene layers were inferred (Fig. 12). At that point the basin has a depth of 8000 m. The Campanian rocks show a recent temperature of ~170 °C and a maturity of ~1.30%VRr. For the Early Miocene rocks a recent temperature of ~80 °C and a maturity of ~0.50%VRr can be inferred. The simulation suggests that the evolution of the Limón fold-and-thrust belt has no significant effect on the thermal field. There is no distortion due to the deformation. The present-day temperature field is characterized by surface-parallel isotherms (Fig. 11).

Comparison of the burial history of the North and South Limón Basin

The software PetroMod® 2D allows the extraction of geohistory curves at any location of the 2D section. This 1D extraction was performed for each sub-basin (Fig. 13a

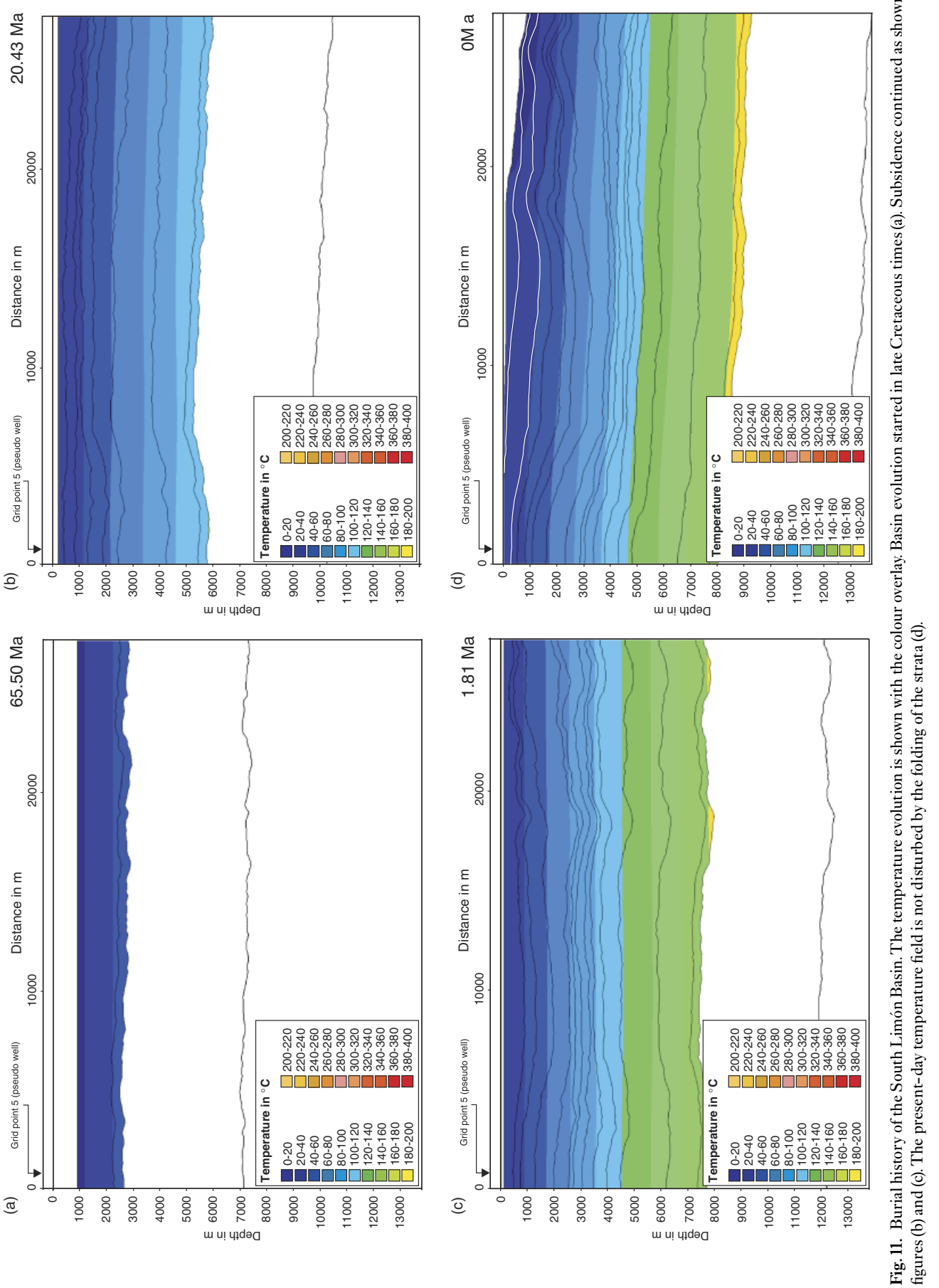

Fig. 11. Burial history of the South Limón Basin. The temperature evolution is shown with the colour overlay. Basin evolution started in late Cretaceous times (a). Subsidence continued as shown in figures (b) and (c). The present-day temperature field is not disturbed by the folding of the strata (d).

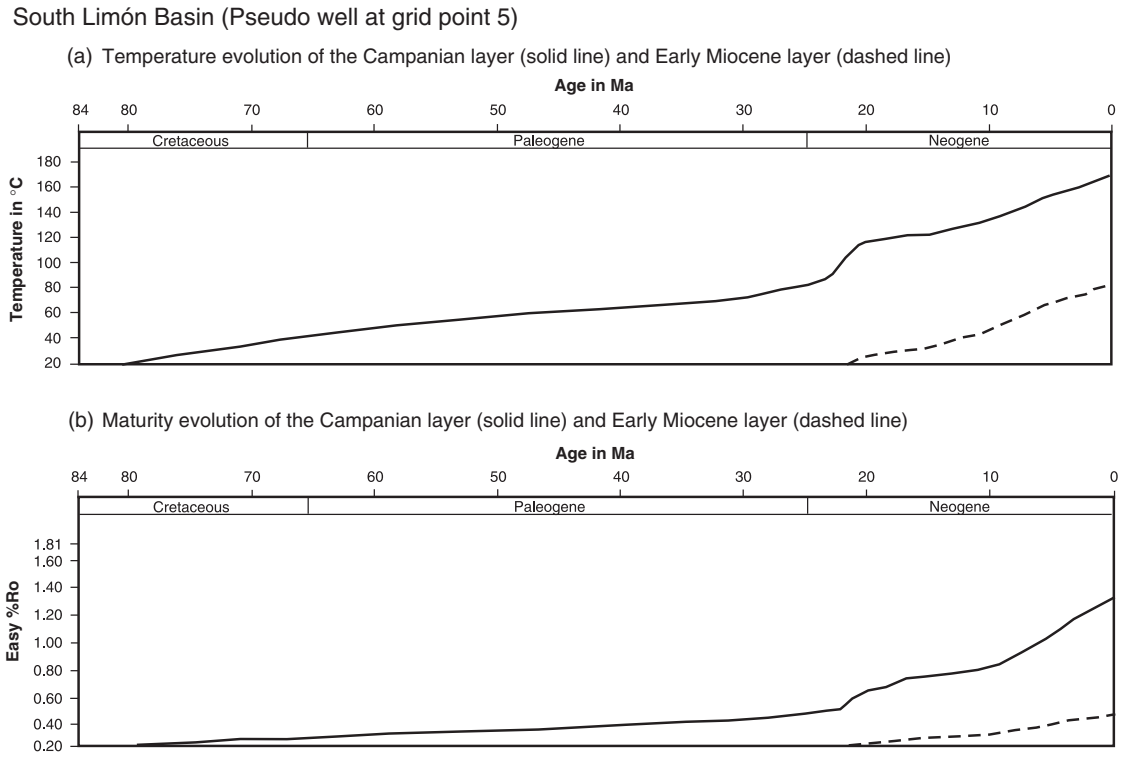

Fig. 12. Temperature and maturity evolution for the Campanian and Early Miocene intervals in the South Limón Basin.

and b). The North Limón Basin is characterized by a subsidence rate of $\sim$68 m m.y.$^{-1}$ during the Palaeocene (Fig. 13a). At the beginning of the Neogene, there is a minor phase of uplift. During the Middle Miocene the subsidence rate is $\sim$300 m m.y.$^{-1}$ Between 6 and 4 Ma another short period of uplift occurred. The last 4 m.y. (Late Pliocene–Pleistocene) show a subsidence of $\sim$200 m m.y.$^{-1}$ In the South Limón Basin the period 66–34 Ma is characterized by a subsidence rate of $\sim$56 m Ma^{-1}. At the beginning of the Neogene there is a distinct change in the trend. The subsidence abruptly increased to $\sim$675 m m.y.$^{-1}$ for a period of approximately 2 m.y. The following 9 m.y. are characterized by a rate of $\sim$150 m m.y.$^{-1}$ The period 12–2 Ma shows a subsidence of 55 m m.y.$^{-1}$; between 2 and 0.5 Ma there is an increase to 280 m m.y.$^{-1}$ During the last 0.5 m.y. there was uplift.

LIMITATIONS OF THE MODELS

The results of the basin modelling must be regarded as an initial work because of the limited data. The vitrinite reflectance measurements were taken from an unpublished report. There is no information provided about the uncertainties of the measurements. In addition, the calibration with one vitrinite profile and a few measurements of the present-day geothermal gradient for each sub-basin led to relatively unconstrained thermal models. Regional predictions are not possible. Nevertheless, the fit of the simulated recent temperature field and the measured bottom-hole temperatures show that the simulations are reasonable at least for the modelled sections.

DISCUSSION

The geological setting of the Limón Basin with the two different sub-basins allows us to study the controlling factors of the basin-system in great detail. Although there are distinct differences in structural style, the burial history curves from the North and South Limón Basins show a linear subsidence trend in pre-Neogene times (Fig. 13a and b). This is probably typical for back-arc basins, which evolved behind island-arcs. There is no evidence for an initial rift-phase during the early stage of basin evolution. The subsidence rate is $\sim$68 to $\sim$56 m Ma^{-1}. This is consistent with Mende's (2001) conclusion that the Limón Basin started as a non-extensional back-arc basin behind the volcanic arc. Mende (2001) observed bimodal volcanism with dyke intrusions and the formation of pillow lavas that he interpreted to be an indicator of a Palaeocene to Eocene rifting event. Such a distinct rift-phase cannot be confirmed with the seismic data or by our basin modelling. The geohistory curve for the onshore South Limón Basin shows a very similar evolution, with an initial linear subsidence trend in pre-Neogene times (Fig. 13b). In contrast to the northern sub-basin, there is a pronounced increase in subsidence (675 m Ma^{-1}) at the beginning of the Neogene. The shape of the burial history curve is consistent with a foreland basin setting (Angevine *et al.*, 1990). The increase in subsidence probably indicates the point when the back-arc basin was transformed into a retro-arc foreland basin. The rapid subsidence is interpreted to have resulted from crustal loading due to the evolution of the Cordillera de Talamanca. The increase at 2 Ma is probably related to the evolution of the Limón fold-and-thrust belt. The

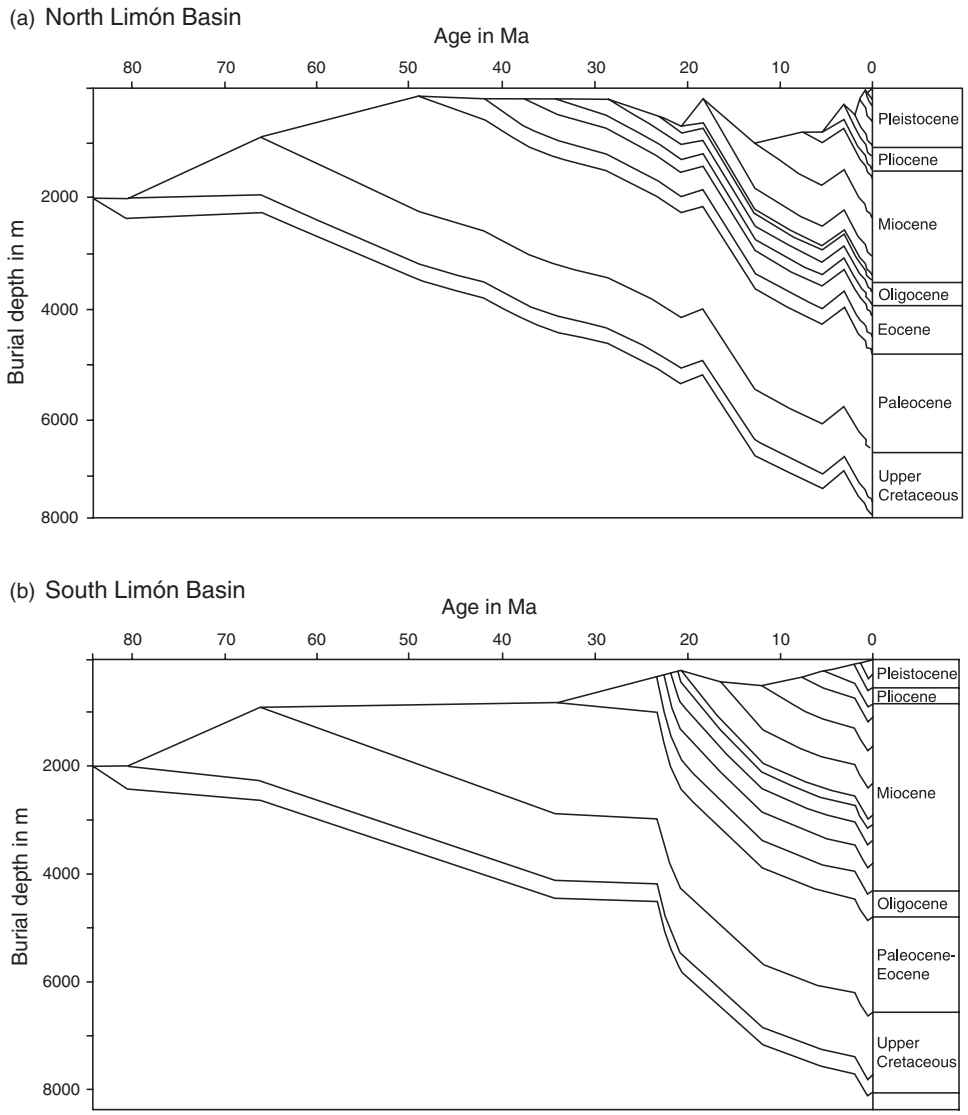

Fig. 13. Comparison of the geohistory curves from the (a) North Limón Basin and (b) South Limón Basin (see text for detailed explanation). The geohistory curve from the North Limón Basin was extracted at grid point 71, and the geohistory curve from the South Limón Basin was extracted at grid point 5.

sediments deposited in the South Limón Basin were successively folded and integrated into the propagating deformed belt. The different Neogene geohistory curves observed in the North and South Limón Basin can clearly be attributed to the different structural settings. The North Limón Basin is a back-arc basin. The South Limón Basin also evolved as a back-arc basin, but in contrast to the northern sub-basin was later compressed and transformed into a fold-and-thrust belt.

The results of the thermal modelling indicate that the North Limón Basin is characterized by a mean heat flow of $60\,mW\,m^{-2}$ and the South Limón Basin by a mean heat flow of $41\,mW\,m^{-2}$. The heat flow in both sub-basins is unusually low compared with other back-arc settings along the eastern Pacific margin (Hyndman *et al.*, 2005). The average heat flow in active back-arc basins is $65–120\,mW\,m^{-2}$ (Allen & Allen, 1992). The geothermal gradient observed in wells in the Limón area is also moderate with $\sim 3\,^{\circ}C\,100\,m^{-1}$. Similar geothermal gradients are observed in the Nicaraguan back-arc (Misquito Basin) (Darce *et al.*, 2000) (Fig. 14). The low heat flow in the North Limón Basin can be explained by the lack of a rift-phase. As mentioned above, there is no evidence for important crustal stretching. Another possible explanation for the low heat flow is given by the nature of the underlying lithosphere. Data of Darce *et al.* (2000) show a decreasing geothermal gradient from 3.5 to $2.5\,^{\circ}C\,100\,m^{-1}$ from north to south in the Misquito Basin (Fig. 14). Munoz *et al.* (1997) concluded that the basement in the Misquito Basin changes from north to south from a continental over transitional to an oceanic crust. In contrast to the continental crust, the oceanic crust has little radiogenic heat production. The crustal variations observed by Munoz *et al.* (1997) may explain the decrease in the geothermal gradient in that area. The basins further to the south in Costa Rica and Panama are exclusively

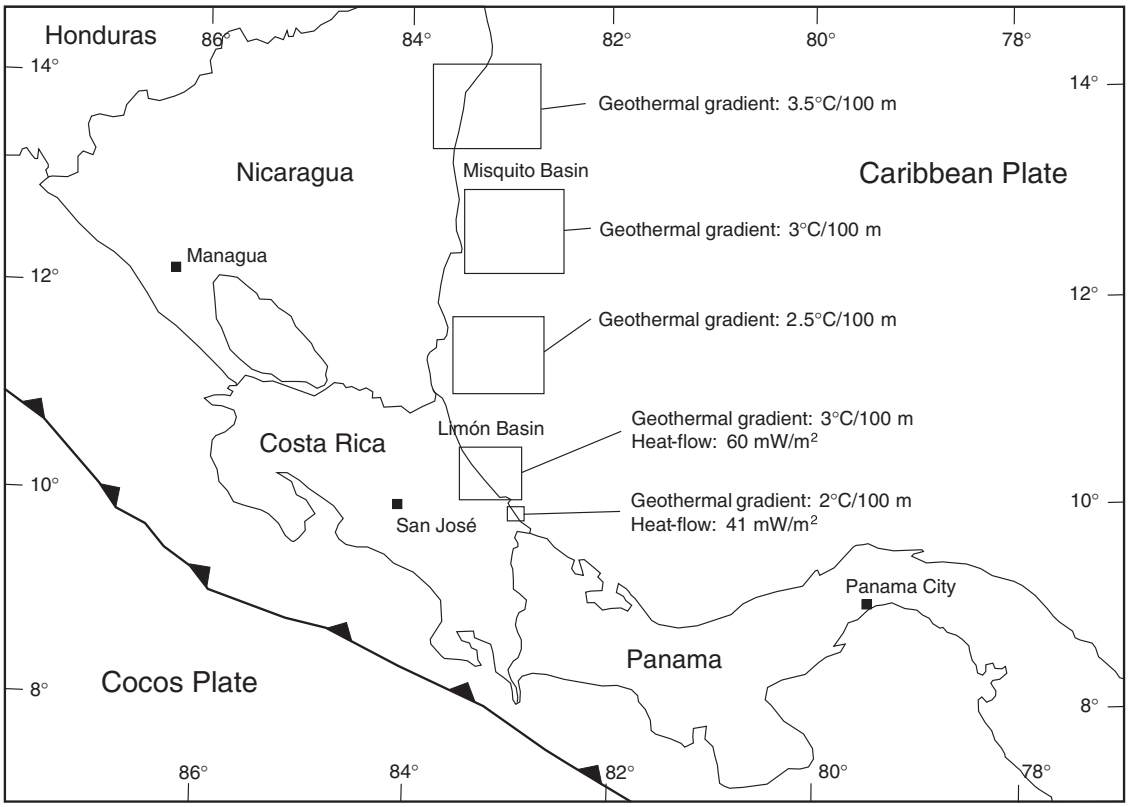

Fig. 14. Geothermal gradient and heat flow in southern Central America. The map is a compilation of data from Astorga *et al.* (1991), Darce *et al.* (2000), and simulation results from this study. The geothermal gradient decreases from north to south in the Misquito Basin (Nicaragua), probably related to a change in crustal structure. The Costa Rican back-arc is characterized by a moderate geothermal gradient of 3 °C 100 m $^{-1}$ in the North Limón area and a lower value of 2 °C 100 m $^{-1}$ in the northeastern part of the Limón fold-and-thrust belt.

underlain by basaltic crust. Radiogenic heat production is absent.

To explain the low heat flow in the Limón Basin, blanketing effects due to high sedimentation rates must also be taken into account. High sedimentation rates can drastically influence the surface heat flow. In the North and South Limón Basin, the Pleistocene sediments reach a thickness of nearly 1 km. Husson & Moretti (2002) pointed out that active sedimentation can reduce the heat flow by a factor of 2 in the uppermost kilometres. In the Gulf of Lyon sedimentation rates of 620 m m.y. $^{-1}$ absorb 32% of the surface heat flow (Lucazeau & Le Douaran, 1985). In the North Limón Basin the sedimentation rates in the Early Pleistocene locally exceed ~1500 m m.y. $^{-1}$ (Fig. 15). In the Late Pleistocene the sedimentation rates are in a range of ~300–1200 m m.y. $^{-1}$ For the South Limón Basin, the piggy-back basins show high sedimentation rates of up to ~1650 m m.y. $^{-1}$ (Fig. 15).

The heat flow on the modelled section from the South Limón Basin between Puerto Limón and Cahuita is significantly lower than the heat flow in the North Limón Basin. This lower heat flow might be a function of the low-angle subduction of the Cocos Plate in the area of southern Costa Rica. As mentioned before the low subduction angle is caused by the bouyant Cocos Ridge, which rests on the Cocos Plate. The Central American subduction zone is characterized by strong along-trench variations in the dip angle of the Wadati-Benioff zone. Protti *et al.* (1995) observed an angle of 84° under Nicaragua, 60° under Central Costa Rica and a flat slab with no Wadati-Benioff zone under South Costa Rica. Following Campos (2001), the subduction angle in southern Costa Rica has shallowed since Middle Oligocene times. As suggested in the model of Gutscher (2002), a low-angle subduction pushes the mantle-wedge backwards, resulting in an increase of the cool fore-arc area. The significant gap in the volcanic chain of the Cordillera de Talamanca has been interpreted to result from the subduction of the Cocos Ridge, which stopped magma production from the mantle-wedge at 8 Ma (Abratis & Wörner, 2001). De Boer *et al.* (1995) proposed a decrease in the subduction angle of the Cocos Plate since Miocene times, in combination with thickening of the upper plate.

Further reasons for the locally low heat flow can probably be found in cooling meteoric waters. The prevailing wind in that area transports water-saturated air from the Caribbean Sea towards the southeast. The Cordillera de Talamanca evolved in Miocene times (Campos, 2001). Since several million years ago, the elevated mountain range has acted as a barrier that induces orographic rain and probably acts as a potential recharge area for groundwater. The topographically low North Limón Basin is probably a discharge area. The strong effect of groundwater flow on the geothermal gradient and heat flow is well

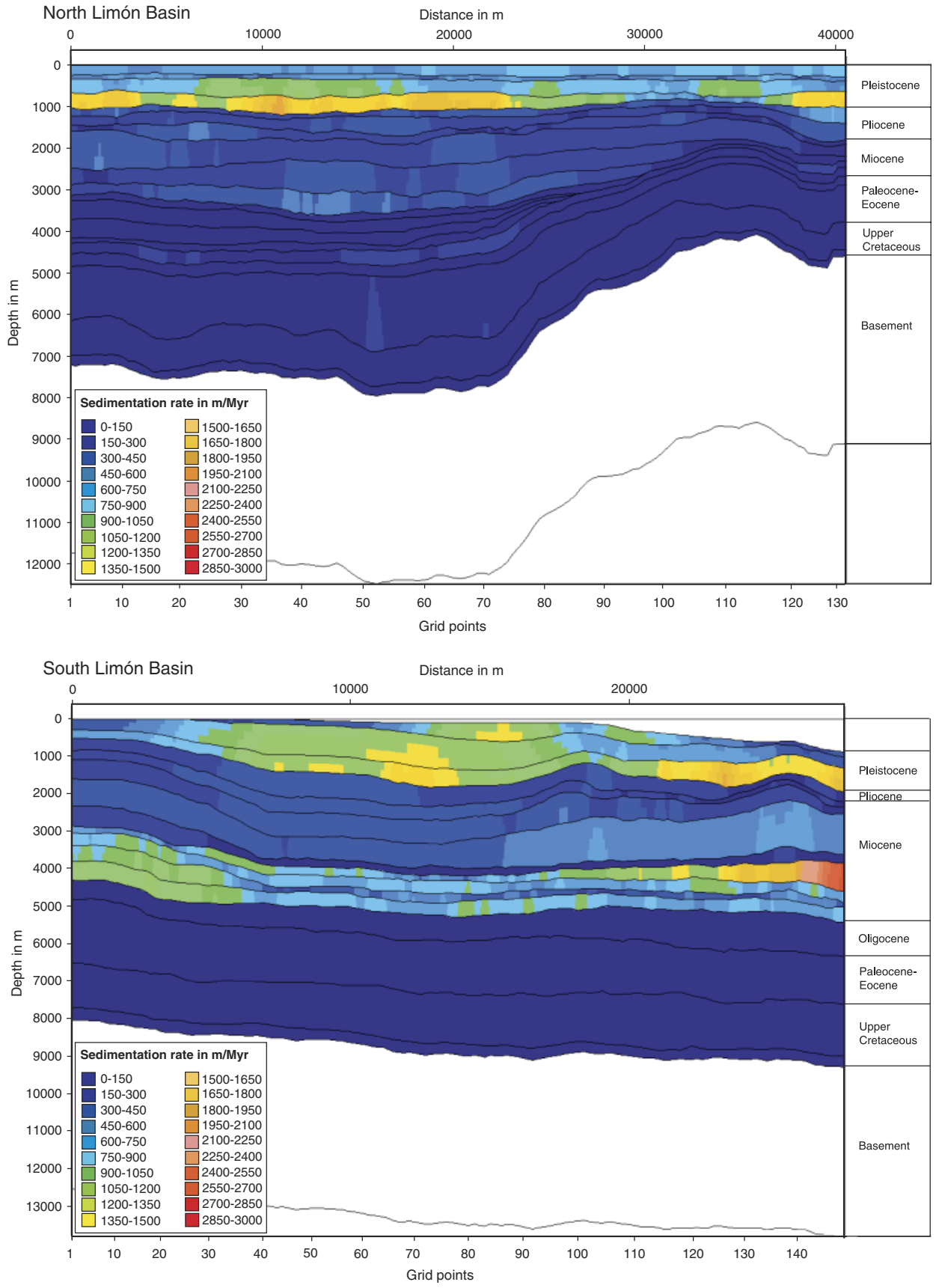

Fig. 15. Sedimentation rates for the North and South Limón Basin. In the North Limón Basin, sedimentation rates of $\sim$1500 m m.y.$^{-1}$ occur in the Pleistocene. In the South Limón Basin, the sedimentation rate in the Pleistocene locally reaches $\sim$1600 m m.y.$^{-1}$ In the North Limón Basin, the high Pleistocene sedimentation rates show a quite uniform distribution along the modelled section, whereas in the South Limón Basin they are restricted to the piggy-back basins.

known from the Rocky Mountain Foothills in Alberta and the Great Plains in the United States (Majorowicz *et al*., 1984, 1985; Gosnold, 1985). Gayer *et al*. (1998) and Nunn *et al*. (2005) have shown the strong impact of a topographically driven downward flow of groundwater on the thermal field of a sedimentary basin. The recharge areas are characterized by a low temperature and the discharge areas show increased values. The calibration well in the South Limón Basin is located relatively close to the possible recharge area and might be influenced by cooling effects. Despite the shaly nature of the Neogene part of the basin fill, the effect of groundwater flow must be taken into account.

Crustal thickening as a consequence of the evolution of the Limón fold-and-thrust belt can be ruled out to explain the low heat flow. The displacement along the thrust faults is very low and has not led to crustal thickening.

Most of the deformation in the offshore part of the Limón fold-and-thrust belt took place in the Pleistocene (Brandes *et al*., in press). Despite this young and rapid deformation, the present-day temperature field is not disturbed. The isotherms are still more or less parallel to the sediment surface. It is assumed that the deformation rate and the wavelength of the anticline structures in the Limón Basin are too low to have an effect. In the Limón Belt, the conductive heat transfer was fast enough to compensate the effect of folding. Husson & Moretti (2002) have shown that even thrusting is very unlikely to disturb the thermal field in fold-and-thrust belts.

CONCLUSIONS

The Limón back-arc basin is an excellent setting to study the evolution of the thermal field and the highly variable heat flow in arc-related sedimentary basins. The burial history curves of the North and South Limón Basin record the different tectonic settings. The pre-Neogene burial history curves from the North and South Limón Basin show a linear subsidence trend. No initial rift-phase can be observed. In the South Limón Basin, the subsidence strongly increased at the beginning of the Neogene. The shape of the burial history curve is similar to foreland basin settings. The abrupt increase in subsidence is interpreted to indicate the point when the back-arc basin was transformed into a retro-arc foreland basin.

Based on the thermal modelling results, it is assumed that the heat flow distribution in arc-related basins is very heterogenous and strongly influenced by a combination of local parameters. The thermal modelling indicates a mean heat flow of $60\,mW\,m^{-2}$ for the North Limón Basin and $41\,mW\,m^{-2}$ for the South Limón Basin. The heat flow is low compared with other back-arc basins in the circum Pacific region. The lower values are attributed to the following effects: (1) underlying basaltic crust, (2) the lack of an initial rift phase, (3) the low extension rates, (4) absence of volcanic activity and (5) insulation effects of a thick sediment pile. Additional reasons for the locally lower heat flow in the southern sub-basin can be found in the subduction geometry. The subduction angle drastically decreases in southern Costa Rica because of the buoyant Cocos Ridge. Owing to the low subduction angle, the cool fore-arc mantle-wedge below the island-arc is pushed backwards, increasing the cooled area. Furthermore, cooling meteoric waters, which probably infiltrate in the Cordillera de Talamanca close to the calibration well of the South Limón Basin, may also reduce the heat flow.

Although there is a rapid deformation in Plio-Pleistocene times, the present-day temperature field is not disturbed by the folding. The heat transfer was fast enough to compensate for the effects of folding. The deformation rate and the wavelength of the anticlinal structures in the Limón Basin are too low to influence the temperature distribution.

ACKNOWLEDGEMENTS

We would like to thank the Costa Rican Ministry of Environment and Energy (MINAE) for providing the data base. We are indebted especially to Alvaro Aguilar and Gustavo Segura for logistic help. Financial support from the German Research Foundation (DFG) Project Wi 1844/6-1 and a graduate scholarship from the University of Hannover are gratefully acknowledged. Many thanks are due to Stefan Back for help with seismic interpretation. We are very grateful to Peter Blisniuk for introduction of the techniques of balanced cross-sections and to Michael Haschke for the discussion about the thermal structure of subduction zones and magmatic arcs. Ulrich Asprion, Franz Binot, Lolita Campos, Christoph Gaedicke, Stefan Ladage, Andreas Mende, Klaus Reicherter and Danny Schwarzer helped with seismic interpretation and basin modelling. Imke Struß is gratefully acknowledged for constructive discussions and help with seismic interpretation and basin modelling. The whole manuscript greatly benefited from careful reviews by Michelle Kominz, Claire Currie and Robert Harris.

REFERENCES

Abratis, M. & Wörner, G. (2001) Ridge collision, slab-window formation, and the flux of Pacific asthenosphere into the Caribbean realm. *Geology*, **29**, 127–130.

Allen, P.A. & Allen, J.R. (1992) *Basin Analysis*. Blackwell, Oxford, 451pp.

Amann, H. (1993) Randmarine und terrestrische Ablagerungsräume des neogenen Inselbogensystems in Costa Rica (Mittelamerika) *Profil*, **4**, 161pp.

Angevine, C.L., Heller, P.L. & Paola, C. (1990) Quantitative sedimentary basin modeling. *AAPG Course Note Ser.*, **32**, 247pp.

Astorga, A. (1988) Geodinámica de las cuencas del Cretácico Superior – Paleógeno de la región "forearc" del Sur de Nicaragua y Norte de Costa Rica. *Rev. Geol. Am. Central*, **9**, 1–40.

Astorga, A. (1997) El puente-istmo de América Central y la evolución de la Placa caribe (con énfasis en el Mesozoico). *Profil*, **12**, 201pp.

Astorga, A., Fernandez, J.A., Barboza, G., Campos, L., Obando, J., Aguilar, A. & Obando, L.G. (1991) Cuencas sedimentarias de Costa Rica: evolucion geodinamica y potencial de hidrocarburos. *Rev. Geol. Am. Central*, **13**, 25–59.

Barboza, G., Barrientos, J. & Astorga, A. (1995) Tectonic evolution and sequence stratigraphy of the central Pacific margin of Costa Rica. *Rev. Geol. Am. Central*, **18**, 43–63.

Barboza, G., Fernández, A., Barrientos, J. & Bottazzi, G. (1997) Costa Rica: petroleum geology of the Caribbean margin. *Lead. Edge*, **16**, 1787–1794.

Barckhausen, U., Ranero, C.R., von Huene, R., Cande, S.C. & Roeser, H.A. (2003) Revised tectonic boundaries in the Cocos Plate off Costa Rica: implications for the segmentation of the convergent margin and for plate tectonic models. *J. Geophys. Res.*, **106**, 19207–19220.

Barrientos, J., Bottazzi, G., Fernández, A. & Barboza, G. (1997) Costa Rican data synthesis indicates oil, gas potential. *Oil Gas J.*, **12**, 76–80.

Bond, G.C., Kominz, M.A. & Sheridan, R.E. (1995) Continental terraces and rises. In: *Tectonics of Sedimentary Basins* (Ed. by C.J. Busby & R.V. Ingersoll), pp. 149–178. Blackwell Science, Oxford.

Bottazzi, G., Fernandez, A. & Barboza, G. (1994) Sedimentología e historia tectono-sedimentaria de la cuenca Limón Sur. In: *Geology of an Evolving Island Arc, The Isthmus of Southern Nicaragua, Costa Rica and Western Panamá* (Ed. by H. Seyfried & W. Hellmann), *Profil*, **7**, 351–389.

Boyer, S.E. & Elliott, D. (1982) Thrust systems. *AAPG Bull.*, **66**, 1196–1230.

Brandes, C., Astorga, A., Back, S., Littke, R. & Winsemann, J. (2007a) Deformation style and basin-fill architecture of the offshore Limón back-arc basin (Costa Rica). *Mar. Petrol. Geol.*, **24**, 277–287.

Brandes, C., Astorga, A., Back, S., Littke, R. & Winsemann, J. (2007b) Fault controls on sediment distribution patterns, Limón Basin, Costa Rica. *J. Petrol. Geol.*, **30**(1), 25–40.

Brandes, C., Astorga, A., Blisniuk, P., Littke, R. & Winsemann, J. (in press) Anatomy of anticlines, piggy-back basins and growth strata: a case study from the Limón fold-and-thrust belt, Costa Rica. *International Association of Sedimentologists Series 38*: Sedimentary Processes, Environments and Basins (Ed. by G. Nichols, F. Williams & C. Paola), pp. 91–110.

Burbridge, D.R. & Braun, J. (2002) Numerical models of the evolution of accretionary wedges and fold-and-thrust belts using the distinct-element method. *Geophys. J. Int.*, **148**, 542–561.

Calvo, C. (2003) Provenance of plutonic detritus in cover sandstones of Nicoya Complex, Costa Rica: cretaceous unroofing history of a Mesozoic ophiolite sequence. *Geol. Soc. Am. Bull.*, **115**, 832–844.

Campos, L. (2001) Geology and basins history of middle Costa Rica: an intraoceanic island arc in the convergence between the Caribbean and the central pacific plates. *Tübinger Geowissenschafiliche Arbeiten*, Reihe A, Band **62**, 138 pp

Coates, A.G., Aubry, M.-P., Berggren, W.A., Collins, L.S. & Kunk, M. (2003) Early Neogene history of the Central American arc from Bocas del Toro, western Panama. *Geol. Soc. Am. Bull.*, **115**, 271–287.

Coates, A.G., Jackson, J.B.C., Collins, L.S., Cronin, T.M., Dowsett, H.J., Bybell, L.M., Jung, P. & Obando, J.A. (1992) Closure of the Isthmus of Panama: the near-shore marine record of Costa Rica and western Panama. *Geol. Soc. Am. Bull.*, **104**, 814–828.

Collins, L.S., Coates, A.G., Jackson, J.B.C. & Obando, J.A. (1995) Timing and rates of emergence of the Limón and Bocas del Toro basins: Caribbean effects of Cocos Ridge subduction? In: *Geologic and Tectonic Development of the Caribbean Plate Boundary in Southern Central America* (Ed. by P. Mann), *Geol. Soc. Am. Spec. Pap.* **295**, 263–289.

Dahlen, F.A. (1984) Noncohesive critical coulomb wedges: an exact solution. *J. Geophys. Res.*, **89**, 10125–10133.

Dahlen, F.A., Suppe, J. & Davis, D. (1984) Mechanics of fold-and-thrust belts and accretionary wedges: cohesive coulomb theory. *J. Geophys. Res.*, **89**, 10087–10101.

Dahlstrom, C.D.A. (1969) Balanced cross-sections. *Can. J. Earthsci.*, **6**, 743–757.

Darce, M., Baca, D., Duarte, M., Barboza, G. & Fernadez, A. (2000) New law, seismic information smooth Nicaragua licensing. *Oil Gas J.*, **14**, 72–74.

Davis, D., Suppe, J. & Dahlen, F.A. (1983) Mechanics of fold-and-thrust belts and accretionary wedges. *J. Geophys. Res.*, **88**, 1153–1172.

De Boer, J.Z., Drummond, M.S., Bordelon, M.S., Defant, M.J., Bellon, H. & Maury, R.C. (1995) Cenozoic magmatic phases of the Costa Rican island arc (Cordillera de Talamanca). In: *Geologic and Tectonic Development of the Caribbean Plate Boundary in Southern Central America* (Ed. by P. Mann), *Geol. Soc. Am. Spec. Pap.,* **295**, 35–55. Boulder, Colorado.

DeMets, C. (2001) A new estimate for present-day Cocos-Caribbean plate motion: implications for slip along the Central American volcanic arc. *Geophys. Res. Lett.*, **28**, 4043–4046.

Dennison, J.M. & Woodward, H.P. (1963) Palinspastic maps of central Appalachians. *AAPG Bull.*, **47**, 666–680.

DePaor, D.G. (1988) Balanced section in thrust belts part 1: construction. *AAPG Bull.*, **72**, 73–90.

Di Marco, G., Baumgartner, P.O. & Channell, J.E.T. (1995) Late cretaceous-early tertiary paleomagnetic data and a revised tectonostratigraphic subdivision of Costa Rica and western Panama. In: *Geologic and Tectonic Development of the Caribbean Plate Boundary in Southern Central America* (Ed. by P. Mann), *Geol. Soc. Am. Spec. Pap.,* **295**, 1–27.

Donnelly, T.W. (1989) Geologic history of the Caribbean and Central America. In: *The Geology of North America – An overview* (Ed. by A.W. Bally & A.R. Palmer), *Geol. Soc. Am. Spec. Pap.* A, 299–321.

Durand, B., Alpern, B., Pittion, J.L. & Pradier, B. (1986) Reflectance of vitrinite as a control of thermal history of sediments. In: *Thermal Modeling in Sedimentary Basins* (Ed. by J. Burrus), *Collect. Colloq. Sémin.*, **44**, 441–474.

Escalante, G. & Astorga, A. (1994) Geología del este de Costa Rica y el norte de Panama. *Rev. Geol. Amér. Central. Vol. esp. Terremoto Limón*, 1–14.

Fernandez, J.A., Bottazzi, G., Barboza, G. & Astorga, A. (1994) Tectónica y estratigrafia de la Cuenca Limón Sur. *Rev. Geol. Am. Central. Vol. esp. Terremoto Limón*, 15–28.

Friberg, L.J. (2001) Untersuchungen zur Temperatur- und Absenkungsgeschichte sowie zur Bildung und Migration von Methan und molekularem Stickstoff im Nordostdeutschen Becken. *Berich. Forschungszentr. Jülich*, **3914**, 248pp.

Frisch, W., Meschede, M. & Sick, M. (1992) Origin of the Central American ophiolites: evidence from paleomagnetic results. *Geol. Soc. Am. Bull.*, **104**, 1301–1314.

Gayer, R., Garven, G. & Ricard, D. (1998) Fluid migration and coal-rank development in foreland basins. *Geology*, **26**, 678–682.

Gosnold, W.D. (1985) Heat flow and ground water flow in the great plains of the United States. *J. Geodyn.*, **4**, 247–264.

Gosnold, W.D. & Fischer, D.W. (1986) Heat flow studies in sedimentary basins. In: *Thermal Modelling in Sedimentary Basins* (Ed. by J. Burrus), *Collect. Colloq. Sémin.*, **44**, 199–217.

Gräfe, K., Frisch, W., Villa, I.M. & Meschede, M. (2002) Geodynamic evolution of southern Costa Rica related to low-angle subduction of the Cocos Ridge: constraints from thermochronology. *Tectonophysics*, **348**, 187–204.

Gutscher, M.A. (2002) Andean subduction styles and their effect on thermal structure and interplate coupling. *J. South Am. Earth Sci.*, **15**, 3–10.

Husson, L. & Moretti, I. (2002) Thermal regime of fold and thrust belts – an application to the Bolivian sub Andean zone. *Tectonophysics*, **345**, 253–280.

Hutchinson, D.R., Grow, J.A., Klitgord, K.D. & Swift, B.A. (1982) Deep structure and evolution of the Carolina Trough. *AAPG Mem.*, **34**, 129–152.

Hyndman, R.D., Currie, C.A. & Mazotti, S.P. (2005) Subduction zone backarcs, mobile belts, and orogenic heat. *GSA Today*, **15**, 4–10.

Jensen, P.K. (1997) Modelling the history of burial, temperature, and hydrocarbon generation of sedimentary basins. Application to the Aars-1A well. *Geophys. Trans.*, **41**, 65–94.

Kolarsky, R.A., Mann, P. & Montero, W. (1995) Island arc response to shallow subduction of the Cocos Ridge, Costa Rica. In: *Geologic and Tectonic Development of the Caribbean Plate Boundary in Southern Central America* (Ed. by P. Mann), *Geol. Soc. Am. Spec. Pap.*, **295**, 235–262.

Krawinkel, J.J. (2003) Struktur und Kinematik am konvergenten Plattenrand der südlichen Zentralamerikanischen Landbrücke (Zentral- und Süd-Costa Rica, West-Panamá). *Profil*, **20**, 36pp.

Krawinkel, J. & Seyfried, H. (1994) A review of plate-tectonic processes involved in the formation of the southwestern edge of the Caribbean Plate. In: *Geology of an Evolving Island Arc, The Isthmus of Southern Nicaragua, Costa Rica and Western Panamá* (Ed. by H. Seyfried & W. Hellmann), *Profil*, **7**, 47–61.

Krawinkel, H., Seyfried, H., Calvo, C. & Astorga, A. (2000) Origin and inversion of sedimentary basins in southern Central America. *Z. Angew. Geol. SH*, **1**, 71–77.

Larter, S. (1989) Chemical models of vitrinite reflectance evolution. *Geol. Rundsch.*, **78**, 349–359.

Lerche, I., Yarzab, R.F. & Kendall, C.G.ST.C. (1984) Determination of paleoheat flux from vitrinite reflectance data. *AAPG Bull.*, **68**, 1704–1717.

Lucazeau, F. & Le Douaran, S. (1985) The blanketing effect of sediments in basins formed by extension: a numerical model. Application to the Gulf of Lion and Viking graben. *Earth Planet. Sci. Lett.*, **74**, 92–102.

Lundberg, N. (1991) Detrital record of the early Central American magmatic arc: petrography of intraoceanic forearc sandstones, Nicoya Peninsula, Costa Rica. *Geol. Soc. Am. Bull.*, **103**, 905–915.

Lutz, R. (2002) Numerische Simulation der Kohlenwasserstoffgenese an der Subduktionszone vor Costa Rica. *Diss. RWTH Aachen*, 120pp.

Lutz, R., Littke, R., Gerling, P. & Bönnemann, C. (2004) 2D numerical modelling of hydrocarbon generation in subducted sediments at the active continental margin of Costa Rica. *Mar. Petrol. Geol.*, **21**, 753–766.

Majorowicz, J.A., Jones, F.W., Lam, H.L. & Jessop, A.M. (1984) The variability of heat flow both regional and with depth in southern Alberta, Canada: effect of groundwater flow? *Tectonophysics*, **106**, 1–29.

Majorowicz, J.A., Jones, F.W., Lam, H.L. & Jessop, A.M. (1985) Terrestrial heat flow and geothermal gradients in relation to hydrodynamics in the Alberta Basin; Canada. *J. Geodynamics*, **4**, 265–283.

Maresch, W.V., Stöckhart, B., Baumann, A., Kaiser, C., Kluge, R., Krückhans-Lueder, G., Brix, M.R. & Thomson, S. (2000) Crustal history and plate tectonic development in the southern Caribbean. *Z. Angew. Geol. SH 1*, 283–290.

Mareschal, J.C. (1987) Subsidence and heat flow in intracontinental basins and passive margins. In: *Sedimentary Basins and Basin-Forming Mechanisms* (Ed. by C. Beaumont & A.J. Tankard), *Can. Soc. Petrol. Geol.*, **12**, 519–527.

McCulloh, T.H. & Naeser, N.D. (1989) Thermal history of sedimentary basins: introduction and overview. In: *Thermal History of Sedimentary Basins* (Ed. by N.D. Naeser & T.H. McCulloh), pp. 1–11. Springer Verlag, New York.

McNeill, D.F., Coates, A.G., Budd, A.F. & Borne, P.F. (2000) Integrated paleontologic and paleomagnetic stratigraphy of the Upper Neogene deposits around Limon, Costa Rica: a coastal emergence record of the Central American Isthmus. *Geol. Soc. Am. Bull.*, **112**, 963–981.

Mende, A. (2001) Sedimente und Architektur der Forearc- und Backarc-Becken von Südost-Costa Rica und Nordwest-Panamá. *Profil*, **19**, 130pp.

Meschede, M. & Frisch, W. (1998) A plate tectonic model for the Mesozoic and Early Cenozoic history of the Caribbean Plate. *Tectonophysics*, **296**, 269–291.

Meschede, M., Frisch, W., Chinchilla Chavez, A.L., López Saborio, A. & Calvo, C. (2000) The plate tectonic evolution of the Caribbean Plate in the Mesozoic and Early Cenozoic. *Z. Angew. Geol. SH 1*, 275–281.

Mitra, S. (1990) Fault-propagation folds: geometry, kinematic evolution, and hydrocarbon traps. *AAPG Bull.*, **74**, 921–945.

Munoz, A., Baca, D., Artiles, V. & Duarte, M. (1997) Nicaragua: petroleum geology of the Caribbean margin. *Lead. Edge*, **16**, 1799–1805.

Nöth, S., Karg, H. & Littke, R. (2001) Reconstruction of Late Palaeozoic heat flows and burial histories at the Rhenohercynian-Subvariscan boundary, Germany. *Int. J. Earth Sci.*, **90**, 234–256.

Nunn, J.A., Hanor, J.S. & Lee, Y. (2005) Migration pathways in the Central North Slope foreland basin, Alaska, USA: solute and thermal constraints on fluid flow simulations. *Bas. Res.*, **17**, 403–416.

Petmecky, S., Meier, L., Reiser, H. & Littke, R. (1999) High thermal maturity in the Lower Saxony Basin: intrusion or deep burial? *Tectonophysics*, **304**, 317–344.

Petzet, G.A. (1998) Costa Rica awards blocks on Caribbean coast. *Oil Gas J.*, **12**, 76–80.

Pindell, J.L., Cande, S.C., Pitman, W.C., Rowley, D.B., Dewey, J.F., Labrecque, J. & Haxby, W. (1988) A plate-kinematic framework for models of Caribbean evolution. *Tectonophysics*, **155**, 121–138.

Poelchau, H.S., Baker, D.R., Hantschel, T., Horsfield, B. & Wygrala, B. (1997) Basin simulation and the design of the conceptual model. In: *Petroleum and Basin Evolution* (Ed. by D.H. Welte, B. Horsfield & D.R. Baker), pp. 3–70. Springer Verlag, Berlin.

Price, R.A. (2001) An evaluation of models for kinematic evolution of thrust and fold belts: structural analysis of a transverse fault zone in the Front ranges of the Canadian Rockies north of Banff, Alberta. *J. Struct. Geol.*, **23**, 1079–1088.

Protti, M., Güendel, F. & McNally, K. (1995) Correlation between the age of the subducting Cocos plate and the geometry of the Wadati-Benioff zone under Nicaragua and Costa Rica.

In: *Geologic and Tectonic Development of the Caribbean Plate Boundary in Southern Central America* (Ed. by P. Mann), *Geol. Soc. Am. Spec. Pap.,* **295**, 309–326.

Radke, M., Horsfield, B., Littke, R. & Rullkötter, J. (1997) Maturation and petroleum generation. In: *Petroleum and Basin Evolution* (Ed. by D.H. Welte, B. Horsfield & D.R. Baker), pp. 169–230. Springer, Berlin.

Ramsey, J.G. & Huber, M.I. (1987) *The Techniques of Modern Structural Geology*, Vol. II. Academic Press, London, 700pp.

Ranero, C.R. & von Huene, R. (2000) Subduction erosion along the Middle America convergent margin. *Nature*, **404**, 748–752.

Ranero, C.R., von Huene, R., Flueh, E., Duarte, M., Baca, D. & McIntosh, K. (2000a) A cross section of the convergent Pacific margin of Nicaragua. *Tectonics*, **19**, 335–357.

Ranero, C.R., von Huene, R., Flueh, E.R., Weinrebe, W., Hinz, K., Leandro, G., Alvarado, G. & Duarte, M. (2000b) Lower plate control on subduction erosion processes along the middle America convergent margin. *Z. Angew. Geol. SH 1*, 291–296.

Rodon, S. & Littke, R. (2005) Thermal maturity in the Central European Basin system (Schleswig-Holstein area): results of 1D basin modelling and new maturity maps. *Int. J. Earth Sci.*, **94**, 815–833.

Rodriguez, J.F.R. & Littke, R. (2001) Petroleum generation and accumulation in the Golfo San Jorge Basin, Argentina: a basin modeling study. *Mar. Petrol. Geol.*, **18**, 995–1028.

Ross, M.I. & Scotese, C.R. (1988) A hierachical tectonic model of the Gulf of Mexico and the Caribbean region. *Tectonophysics*, **155**, 139–168.

Schmidt, F. & Erdogan, L.T. (1993) Basin modelling in an overthrust area of Austria. In: *Basin Modelling: Advances and Applications* (Ed. By A.G. Doré), *NPF Spec.Publ.*, **3**, 573–581.

Schneider (2003) Basin modeling in complex area: examples from eastern Venezuelan and Canadian foothills. *Rev. IFP*, **58**, 313–324.

Seyfried, H., Astorga, A., Amann, H., Calvo, C., Kolb, W., Schmidt, H. & Winsemann, J. (1991) Anatomy of an evolving Island Arc: tectonic and eustatic control in the south Central American forearc area. In: *Sea-Level Changes at Active Plate Margins: Processes and Products* (Ed. by D.I.M. MacDonald), *Int. Assoc. Sediment. Spec. Publ.,* **12**, 273–292.

Sheehan, C.A., Penfield, G.T. & Morales, E. (1990) Costa Rica geologic basins lure wildcatters. *Oil Gas J.*, **30**, 74–79.

Silver, E.A., Galewsky, J. & McIntosh, K.D. (1995) Variation in structure, style, and driving mechanism of adjoining segments of the North Panama deformed belt. In: *Geologic and Tectonic Development of the Caribbean Plate Boundary in Southern Central America* (Ed. by P. Mann), *Geol. Soc. Am. Spec. Pap.,* **295**, 309–326.

Sleep, N.H. (1979) A thermal constraint on the duration of folding with reference to Acadian geology, New England (USA). *J. Geol.*, **87**, 583–589.

Suppe, J. (1983) Geometry and kinematics of fault-bend folding. *Am. J. Sci.*, **283**, 684–721.

Suppe, J. & Medwedeff, D.A. (1990) Geometry and kinematics of fault-propagation folding. *Eclogae Geol. Helv.*, **83**, 409–454.

Sweeney, J.J. & Burnham, A.K. (1990) Evaluation of a simple model of vitrinite reflectance based on chemical kinetics. *AAPG Bull.*, **74**, 1559–1570.

Taylor, G.H., Teichmüller, M., Davis, A., Dissel, C.F.K., Littke, R. & Robert, P. (1998) *Organic Petrology*. Borntraeger, Berlin, 704pp.

Ungerer, P., Burrus, J., Doligez, B., Chenet, P.Y. & Bessis, F. (1990) Basin evaluation by integrated two-dimensional modeling of heat transfer, fluid flow, hydrocarbon generation and migration. *AAPG Bull.*, **74**, 309–335.

Vergés, J., Muñoz, J.A. & Martínez, A. (1992) South Pyrenean fold and thrust belt: the role of foreland evaporitic levels in thrust geometry. In: *Thrust Tectonics* (Ed. K.R. McClay), pp. 255–263. Chapman and Hall, London, UK.

von Huene, R. & Flüh, E. (1994) A review of marine geophysical studies along the Middle America Trench off Costa Rica and the problematic seaward terminus of continental crust. In: *Geology of an Evolving Island Arc, The Isthmus of Southern Nicaragua, Costa Rica and Western Panamá* (Ed. by H. Seyfried & W. Hellmann), *Profil*, **7**, 143–159.

Walther, C.H.E. (2003) The crustal structure of the Cocos ridge of Costa Rica. *J. Geophys. Res.*, **108**, 1–21.

Weinberg, R.F. (1992) Neotectonic development of western Nicaragua. *Tectonics*, **11**, 1010–1017.

Welte, D.W. & Yalcin, M.N. (1987) Basin modeling – A new comprehensive method in petroleum geology. *Adv. Org. Geochem.*, **13**, 1–3.

Welte, D.H. & Yükler, M.A. (1981) Petroleum origin and accumulation in basin evolution – a quantitative model. *AAPG Bull.*, **65**, 1387–1396.

Werner, R., Hoernle, K., van den Bogaard, P., Ranero, C. & von Huene, R. (1999) Drowned 14-m.y.-old Galápagos archipelago off the coast of Costa Rica: implications for tectonic and evolutionary models. *Geology*, **27**, 499–502.

Weyl, R. (1980) *Geology of Central America*. Borntraeger, Berlin, 371pp.

Wilkerson, M.S. & Dicken, C.L. (2001) Quick-look techniques for evaluating two-dimensional cross sections in detached contractional settings. *AAPG Bull.*, **85**, 1759–1770.

Winsemann, J. (1992) Tiefwasser-Sedimentationsprozesse und -produkte in den Forearc-Becken des mittelamerikanischen Inselbogensystems: eine sequenzstratigraphische Analyse. *Profil*, **2**, 218pp.

Winsemann, J. & Seyfried, H. (1991) Response of deep-water forearc systems to sea-level changes, tectonic activity and volcaniclastic input in central America. In: *Sea-Level Changes at Active Plate Margins: Processes and Products* (Ed. by D.I.M. MacDonald), *Int. Assoc. Sediment. Spec. Publ.*, **12**, 217–240.

Wygrala, B.P., Yalcin, M.N. & Dohmen, L. (1990) Thermal histories and overthrusting–application of numerical simulation technique. *Org. Geochem.*, **16**, 267–285.

Yahi, N., Schäfer, R.G. & Littke, R. (2001) Petroleum generation and accumulation in the Berkine basin, eastern Algeria. *AAPG Bull.*, **85**, 1439–1467.

Yalcin, M.N. (1991) Basin modelling and hydrocarbon exploration. *J. Petrol. Sci. Eng.*, **5**, 379–398.

Yalcin, M.N., Littke, R. & Sachsenhofer, R.F. (1997) Thermal history of sedimentary basins. In: *Petroleum and Basin Evolution* (Ed. by D.H. Welte, B. Horsfield & D.R. Baker), pp. 71–167. Springer, Berlin.

Zhou, Y. & Littke, R. (1999) Numerical simulation of the thermal maturation, oil generation and migration in the Songliao basin, Northeastern China. *Mar. Petrol. Geol.*, **16**, 771–792.

Manuscript received 22 February 2006; Manuscript accepted 12 October 2007.

